Journal Pre-proofs

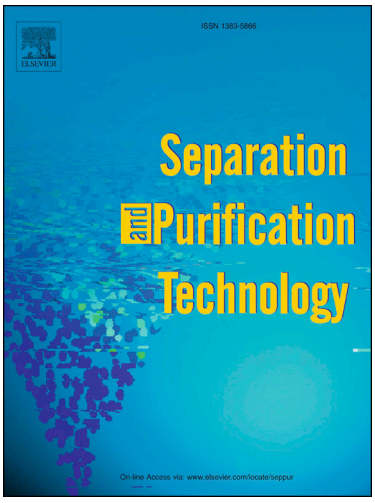

Controlled synthesis of porous Zn/Fe based layered double hydroxides: Synthesis mechanism, and ciprofloxacin adsorption

Shweta Sharma, Gaurav Sharma, Amit Kumar, Pooja Dhiman, TahaniSaad AlGarni, Mu. Naushad, ZeidA. ALOthman, Florian J. Stadler

PII: S1383-5866(21)01189-8
DOI: https://doi.org/10.1016/j.seppur.2021.119481
Reference: SEPPUR 119481

To appear in: *Separation and Purification Technology*

Received Date: 22 June 2021
Revised Date: 6 August 2021
Accepted Date: 11 August 2021

Please cite this article as: S. Sharma, G. Sharma, A. Kumar, P. Dhiman, T. AlGarni, Mu. Naushad, ZeidA. ALOthman, F.J. Stadler, Controlled synthesis of porous Zn/Fe based layered double hydroxides: Synthesis mechanism, and ciprofloxacin adsorption, *Separation and Purification Technology* (2021), doi: https://doi.org/10.1016/j.seppur.2021.119481

Controlled synthesis of porous Zn/Fe based layered double hydroxides: Synthesis mechanism, and ciprofloxacin adsorption

Shweta Sharma[1], Gaurav Sharma[1,2*,3,4], Amit Kumar[1,2], Pooja Dhiman[1], TahaniSaad AlGarni[3], Mu. Naushad[3], ZeidA. ALOthman[3], Florian J. Stadler[2]

CRediT authorship contribution statement

Shweta Sharma: Writing – original draft, Validation, Investigation, Data curtion, **Gaurav Sharma:** Data curation, Conceptualization, Validation, Supervision, Writing – original draft, review & editing. **Amit Kumar:** Writing – original draft, Writing – review & editing. **Pooja Dhiman:** Writing – review & editing. **Tahani Saad AlGarni:** Writing – review & editing. **Mu. Naushad:** Resources, Writing – review & editing. **Zeid A. ALOthman**: Writing – review & editing. **Florian J. Stadler**: Writing – review & editing.

[1]International Research Centre of Nanotechnology for Himalayan Sustainability (IRCNHS), Shoolini University, Solan 173212, Himachal Pradesh, India

[2]College of Materials Science and Engineering, Shenzhen Key Laboratory of Polymer Science and Technology, Guangdong Research Center for Interfacial Engineering of Functional Materials, Nanshan District Key Lab. for Biopolymers and Safety Evaluation, Shenzhen University, Shenzhen 518060, PR China

[3]Department of Chemistry, College of Science, King Saud University, Bldg.#5, Riyadh, Saudi Arabia

[4] School of Science and Technology, Glocal University, Saharanpur, India

Corresponding Author: gaurav8777@gmail.com

Graphical Abstract

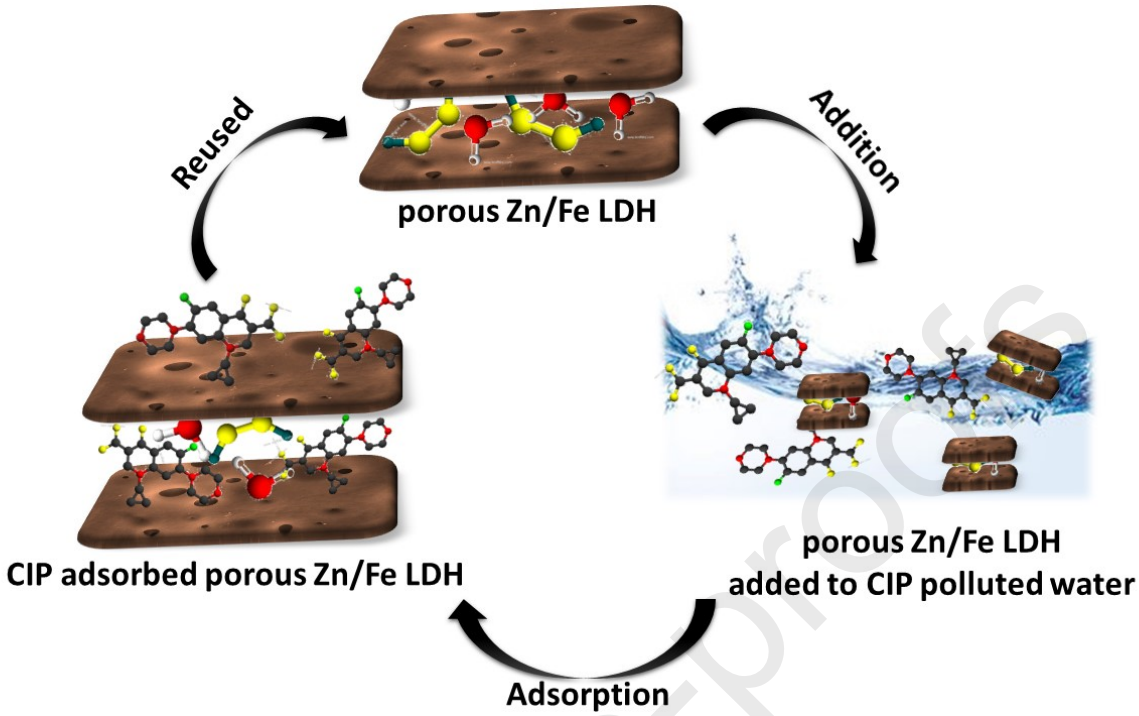

Highlights

- porous Zn/Fe LDH exhibited appreciable adsorption capacity.
- Successful decomposition of H_2O_2 present between the LDH layers.
- Introduction of pores in the layers enhanced the surface area and adsorption activity.
- Successfully reusable for consecutive 6 cycles adsorption cycles.

Abstract

Present work include the designing of a novel porous Zn/Fe layered double hydroxide (LDH) based adsorbent using a combination of three methods, namely, co-precipitation, hydrothermal, and thermal treatment. The Zn/Fe LDH was synthesized by co-precipitation followed by hydrothermal method. The LDH was then intercalated with H_2O_2 and its decomposition under the thermal treatment created oxygen bubbles that pierce holes in the layered structure of the LDH by local pressure build-up. Major techniques used for assessing the morphology and surface area characteristics of the LDH and porous LDH were Scanning electron microscope (SEM) and Brunauer-Emmet-Teller (BET). The intercalation of H_2O_2 and later decomposition triggered by thermal treatment lead to the introduction of pores in the LDH layers that increased the surface area from 108.863 m^2/g to 168.923 m^2/g. The synthesized adsorbent was utilized for the removal of an antibiotic; ciprofloxacin (CIP) from the aqueous solution. The porous Zn/Fe LDH adsorbent was featured with an admirable CIP adsorption capacity of 344.83 mg/g at pH 6.5 and temperature 298 K. The adsorption of CIP onto porous Zn/Fe LDH adsorbent followed the Freundlich isotherm model and pseudo-second-order kinetic model. The temperature increase negatively affected the adsorption rate. The adsorption mechanism of CIP onto porous Zn/Fe LDH was also projected and established, and Cπ- metal interactions, hydrogen bonding, and electrostatic interactions, were found to be the major interactive forces. The thermodynamic study revealed the exothermic and spontaneous nature of the adsorption experiments. Overall, the synthesized adsorbent is sustainable in terms of its usability and non-toxic nature.

Highlights

- Novel porous Zn/Fe based LDH was designed by decomposition of intercalated H_2O_2.
- Effect of solution pH and ionic strength were investigated in detail.
- Introduction of pores in the layers enhanced the surface area and adsorption activity.
- Porous structure of Zn/Fe LDH showed high adsorption capacity of 344.83 mg/g.
- Cπ- metal interactions, hydrogen bonding, and electrostatic interactions were involved in the adsorption.

Keywords: LDH; H_2O_2 intercalation; Porous; Adsorption; Ciprofloxacin.

Graphical Abstract

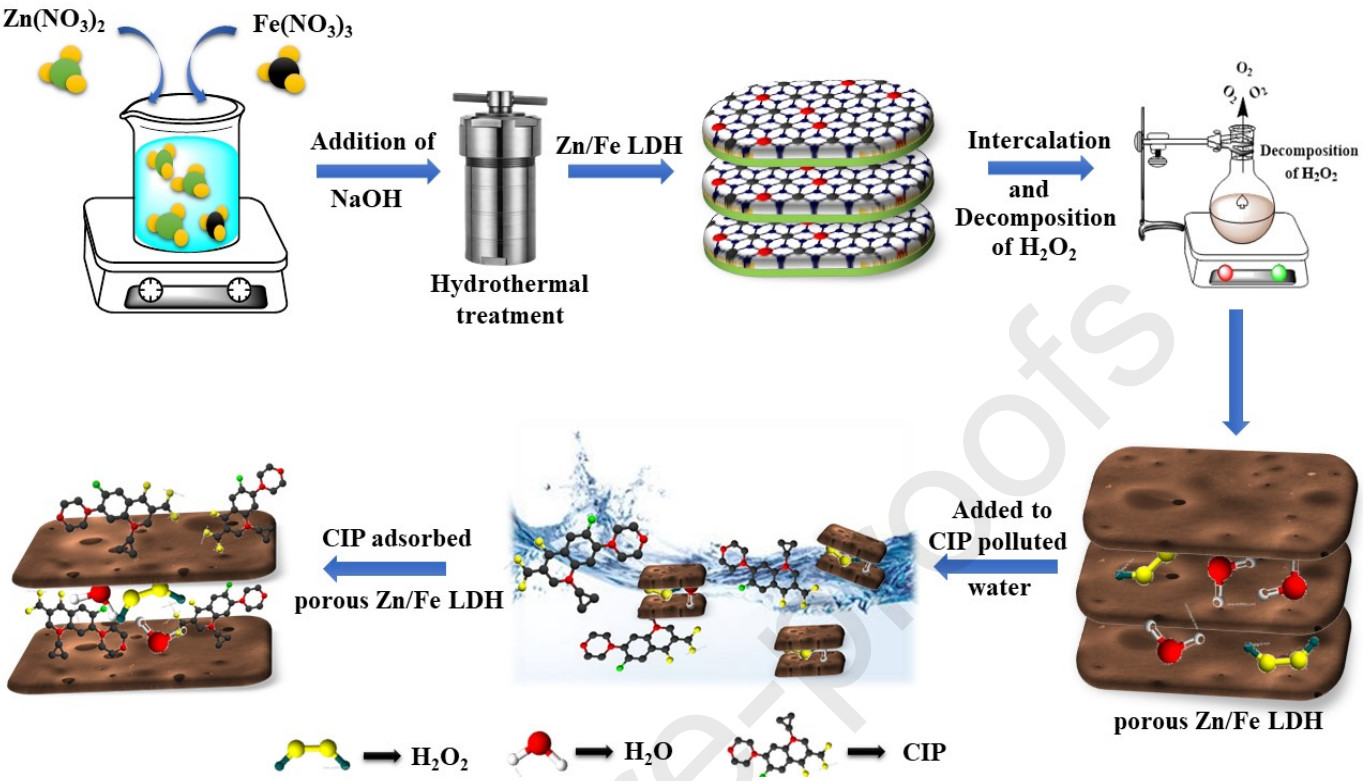

1. Introduction

Uncontrolled discharge of organic effluents such as personal care products, dyes, halogenated flame retardants, pesticides, surfactants, and pharmaceuticals in the water system has triggered public anxieties. Among pharmaceuticals, antibiotics help humans and animals to resist microbial infections [1, 2]. Widespread usage of antibiotics has resulted in their frequent detection in wastewater treatment plants around the world. The presence of pharmaceutical and dyes effluent in wastewater possess many serious environmental issues. It is hazardous not only to aquatic species but also to the human race [3-5]. In the present study, we have focused on the presence of ciprofloxacin (CIP) in the water system and its probable removal by adsorption. CIP is a fluoroquinolone-based antibiotic having antibacterial properties. Its general structural characteristics include a molecular weight of 331.34 g/mol, the melting point of 268°C, the molecular size of 1.31Å× 8.2 Å× 2.5 Å, and pka values 5.9 (pka_1) and 8.9 (pka_2) [6]. It consists of an alkylamine, 1 carboxylic acid, and 2 arylamine groups [7] and thus exhibits both acidic and basic characteristics. Just like other antibiotics, CIP is also resistant to biodegradation and thus poses serious toxic issues to different species.

Adsorption seems to be quite an attractive way of eliminating CIP from the aqueous system. The major positive aspect of this method is that it provides the best results and does not cause any secondary pollution [8-10]. Numerous well-recognized conventional adsorbents are being employed for the removal of various pollutants from the water system such as activated carbon, metal oxides, hydrogels, zeolites, metal- organic frameworks, polymeric materials, bentonite, and nanocomposites [11-17]. Inspite of such of high utilization, there are some drawbacks linked to them such as low adsorption proficiency, low recyclability, and high specificity. So, researchers are in the thrust of developing new materials that have high adsorption rate, good reusability, and with broad spectrum adsorption ability to combat the conundrum of toxic effluents in wastewater [18, 19].

Layered double hydroxides (LDHs) are the layered structures having positively charged bimetal hydroxide layers intercalated with water molecules, hydroxide groups, and anions (carbonate, nitrates and organic compounds, etc) [20]. The general chemical formula representing its structural arrangement is $[M(II)_{1-x}^{2+}M(III)_x^{3+}(OH)_2]^{x-}A_{x/n}^{n-}\cdot mH_2O$ (x represents the ratio of two metal cations $(M(III)^{3+}/(M(II)^{2+} + M(III)^{3+}))$, where n denotes charge on the anion A, and m denotes the number of water molecules present in the interlayer space [21]. LDHs have attractive properties including anion exchange, appreciable chemical stability, compositional diversity, and eco-friendly nature, etc [22]. Besides, the presence of hydroxyl groups on the ionic surface and positive charge on the LDH layers, marks their utilization in various application fields such as photochemistry, environmental remediation, catalysis, polymer additives, and biomedical [23]. Various techniques have been reported in the literature for the synthesis of LDHs such as hydrothermal, co-precipitation, urea hydrolysis, ion exchange, and reconstruction, etc [24]. The most common and facile method is co-precipitation and hydrothermal. In co-precipitation, the two metal salts of pre-decided ratio are mixed with the alkali solution so to acquire the required pH value which aids the precipitation of two metals in the form of metal hydroxide layer intercalated with anions [25]. The hydrothermal treatment helps in producing highly crystalline arrangements [26].

Considering the above presented requirements, we have tried to design an adsorbent having high surface area, porosity as well as functionality that would aid the adsorption application. In the same context, we chose Zn/Fe layered double hydroxides (LDHs) as the basic unit that will provide the

surface area and high functionality. By utilizing the "memory effect" of the LDHs [27], we will intercalate Zn/Fe LDH with H_2O_2. The low thermal stability of H_2O_2 will be used for generating the porous LDH system. So, the presented study is mainly emphasized on the following major objectives: (i) to synthesize Zn/Fe LDH and porous Zn/Fe LDH; (ii) characterization using various techniques, (iii) adsorption of CIP from aqueous solution and to develop its mechanism, and (v) to test the adsorption ability towards other pollutants.

2. Material and methodology

2.1 Chemicals used

The chemicals used in the present study with their purity details are given in Supplementary file as Text S1.

2.2 Synthesis

2.2.1 Synthesis of Zn/Fe LDH

Herein, we used the coprecipitation method followed by hydrothermal treatment for the synthesis of Zn/Fe LDH. In a typical process, 30 mL ferric nitrate and zinc nitrate solutions were prepared in which molar ratio was fixed at 1:4. The solution was continuously stirred for 2 hrs to get a homogeneous solution. For complete precipitation, pH of the solution was adjusted to 9.5 using 0.1M NaOH or HCl solution and was properly mixed for 1 hr. Then, the mixture was transferred to hydrothermal autoclave and treated at 110°C for 10 hrs. After naturally cooling the autoclave to room temperature, the obtained precipitates were washed multiple times with double distilled water till the solution pH became neutral and then dried in a hot air oven at 40°C for 18 hrs.

2.2.2 Synthesis of porous Zn/Fe LDH

For the intercalation of H_2O_2, the memory effect was used. Firstly, the above synthesized Zn/Fe LDH was thermally treated at 400°C for 5 hrs. The formed mixed metal oxides were then used for the intercalation of H_2O_2 into the interlayers of Zn/Fe. Typically, 100 mg of mixed metal oxides were added into 20 mL of 30% H_2O_2 and stirred under dark conditions for 6 hrs in an ice bath. After the successful intercalation, the mixture was then thermally treated at 40°C for 1 hr. It was then filtered and dried at room temperature for 1 complete day that yielded porous Zn/Fe LDH.

2.3 Instrumentation

The instrumentation details are presented in Supplementary file as Text S2.

2.4 Adsorption studies

Batch method was used to carry out the adsorption experiments by mixing 20 mg porous Zn/Fe LDH in the 50 mg/L CIP solution. For the isotherm studies, the adsorbent was immersed into solutions of varying CIP concentrations (10- 100 mg/L) at different temperatures (298, 308, and 318 K) and stirred in a thermostatic shaker at 100 rpm for 10 hrs to achieve equilibrium point. Afterward, the solution was centrifuged and CIP concentration was determined using UV-Vis double beam spectrophotometer at a wavelength of 272 nm. For adsorption kinetics, a CIP solution of concentration 50 mg/L was prepared and 15 mg porous Zn/Fe LDH was added and placed in a thermostatic shaker at 100 rpm. Aliquots were analyzed at different time intervals ranging from 10- 360 min. Equations used for the adsorption amount and adsorption percentage calculations are given in Supplementary file as Text S3 [28] and the recyclability details as Text S4.

3. Results and Discussions

3.1 Synthesis mechanism

Herein, we firstly synthesized Zn/Fe LDH using co-precipitation followed by hydrothermal method. The two metal salt solutions were mixed using vigorous stirring so to form a homogeneous solution. NaOH solution was then added to the metal salt solution so to initiate the co-precipitation process. The desired pH of 10±0.10 was adjusted to ensure complete precipitation. It was followed by the hydrothermal treatment that helped in increasing the crystallinity of Zn/Fe LDH. The metal cation ratio, x is usually found to be between $0.2 \leq x \geq 0.33$ and increase above the value indicates the presence of high charge on the layers and consequently low interlayer distance [29]. In the present study, the ratio of Zn^{2+} and Fe^{3+} selected was 0.2 so that the functionalization and intercalation of H_2O_2 would be easy. After drying, formed Zn/Fe LDH was calcined and then immersed in the H_2O_2 solution under dark conditions. Using the memory effect of LDHs, layered structure was formed intercalated with water and H_2O_2 molecules. After the intercalation, thermal treatment to the H_2O_2 intercalated Zn/Fe LDH resulted in the decomposition of H_2O_2 into O_2 and water molecules. Under the pressure of water molecules, the upward or downward movement of O_2 molecules resulted in the formation of pores in the LDH layers and ultimately the desired porous Zn/Fe LDH [30]. The pressure exerted by oxygen molecules was high enough to form holes in the

layers of Zn/Fe LDH. According to a study presented in 2007 that elaborated the strength of LDH layers, the Young's moduli for hydrated system and isolated nanosheets was 63.4 ± 0.5 GPa and 139 ± 1 GPa, respectively [31]. The overpressure of formed O_2 molecules was high enough that it formed pores in the layers as confirmed by SEM images and they also contributed to the enhancement of interlayer distance which was confirmed by XRD results. In addition, the surface properties such as surface area and pore size were also altered that were determined using BET study which also supported the presented mechanism.

Besides, the complete synthesis mechanism of Zn/Fe LDH was also studied with the help of Zeta potential. Various aliquots were taken at different time intervals during the synthesis and used for generating the probable formation mechanism. Major mechanisms involved in the synthesis of Zn/Fe LDH were; nucleation and precipitation [32, 33]. The Zeta potential values were different at various time intervals that helped in structuring the probable LDH formation steps as shown in Figure 1. During the initial time (Up to 60 minutes), the potential was quite low indicating the nucleation process. This indicates the formation of quite unstable particles in the initial stage. However, after the hydrothermal treatment, the potential of the particles increased indicating the initiation of the crystallization process. The positive potential value during hydrothermal treatment indicate the increased stability of the particles [34]. It is also consistent with the increased positive charge on the LDH layer due to the substitution of Zn^{2+} by Fe^{3+} ions. Also, the potential increased at quite a lower rate suggesting the increasing crystallinity over time which helped in the uniform distribution of Fe^{3+} ions into the layers and ultimately affected the charge density. The hydrothermal treatment promotes the two processes, namely (a) atomic rearrangement so to form crystalline LDH particles, and (b) coarsening process via a surface dissolution of Zn^{2+} and Fe^{3+} ions having high surface energy followed by reprecipitation of Zn^{2+} and Fe^{3+} species. After the complete crystallization of the ions in LDH form, the dissolution of the Zn^{2+} and Fe^{3+} species decreases significantly due to the lower solubility of crystalline LDH particles. Scheme 1 shows the complete synthesis procedure w.r.t. SEM images and crystallinity.

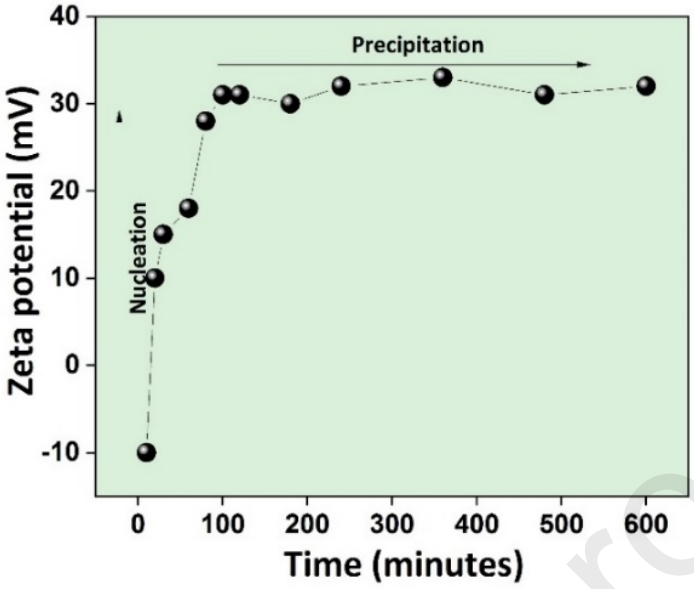

Figure 1. Zeta potential at various time intervals during the synthesis of Zn/Fe LDH

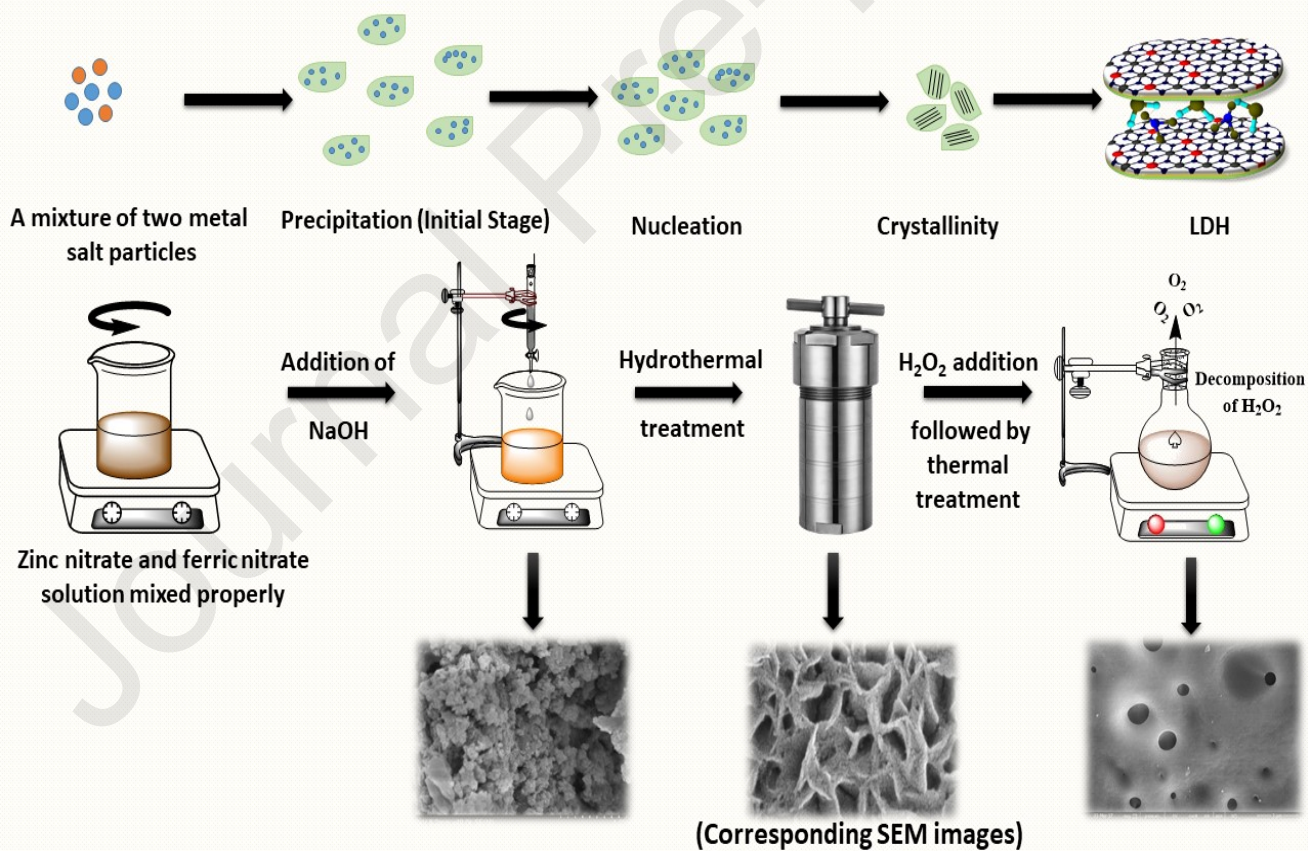

Scheme 1. Schematic presentation for the synthesis of Zn/Fe LDH and porous Zn/Fe LDH

3.2 Characterization

The X-ray diffraction patterns of Zn/Fe LDH, mixed metal oxides, and porous Zn/Fe LDH are shown in Figure 2. The Zn/Fe LDH showed prominent reflections of (003), (006), (018), and (113) which correspond to the characteristic layered arrangement of the formed material [35, 36]. The d- spacing or the interlayer spacing as obtained was 8.61 Å which is in agreement with the data presented in literature [37]. Since the characteristic nucleation and precipitation practices were carried out in a very controlled manner by the slow addition of NaOH, the formation of free $M(OH)_3$ as the by-product was not observed. This is suggestive of the fabrication of a well crystallized Zn/Fe LDH structure. The thermally treated Zn/Fe LDH got converted into mixed oxides as is evident from the results. The layered structure was completely destroyed and metal oxides of Fe and Zn were formed. The characteristic peaks for ZnO were observed at 32.09˚ (100) and 36.86˚ (101) corresponding to hexagonal ZnO (PDF 00-036-1451) [21, 38] and for FeO, peak at 34.36° was obtained that corresponded to the (311) diffraction plane (JCPDS files no. 89-8104) [39]. Immersion of thermally treated Zn/Fe mixed oxides into H_2O_2 resulted in the attainment of layered structure based on the "memory effect" of LDHs. The porous Zn/Fe LDH showed the attainment of layered structure that was confirmed by the appearance of diffraction planes of (003) and (006). The absence of broad background, characteristic of amorphous structures removes the possibility of dissolution of the LDH and formation of amorphous LDH.

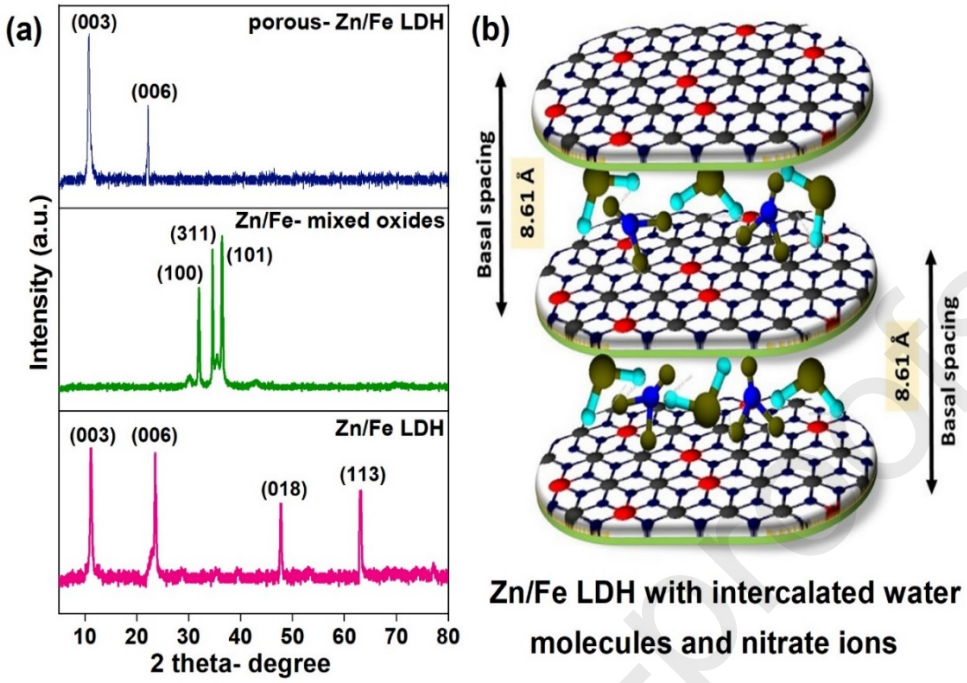

Figure 2. (a) XRD pattern of Zn/Fe LDH, Zn/Fe- mixed oxides, and porous Zn/Fe LDH; and (b) Pictorial presentation of Zn/Fe LDH intercalated with water molecules and nitrate ions with marked basal spacing

The morphological elucidations of the synthesized units were carried out using SEM and obtained results are presented in Figure 3 (a-f). The layered structure of Zn/Fe LDH as shown in Figure 3(a-c) is visible. They exhibited hierarchically morphology designed by the assembly of various small nanosheets. The sheets have irregular size and showed agglomeration. Further magnification of Zn/Fe LDH showed that the nanosheets were ultrathin (Figure 3 (c)). The layered arrangement had probably resulted in high surface area. The EDX spectrum of Zn/Fe LDH is given in the Supplementary file as Figure S1 which confirmed the presence of required elements. Also, the weight % ratio of Fe and Zn was found to be approximately 1:4. The calcination destroyed the layered arrangement and resulted in the formation of mixed Zn/Fe metal oxides. These were obtained in a highly agglomerated form as shown (Figure 3(d)). The porous Zn/Fe LDH showed completely different morphology with pores created in the layers due to the sudden release of O_2 nano-bubbles formed by the decomposition of H_2O_2 in the interlayer region. These are indicative of the production of required pressure by the decomposition that formed the pores in the layer. TEM was employed for the topological analysis of porous Zn/Fe LDH. The pores formed during

thermal treatment are marked in Figure 3(g) and Figure 3(h) shows the HR-TEM image of porous Zn/Fe LDH that depicts the presence of multi-components. Besides, the SAED image (Figure 3(i)) revealed the polycrystalline nature of the synthesized adsorbent.

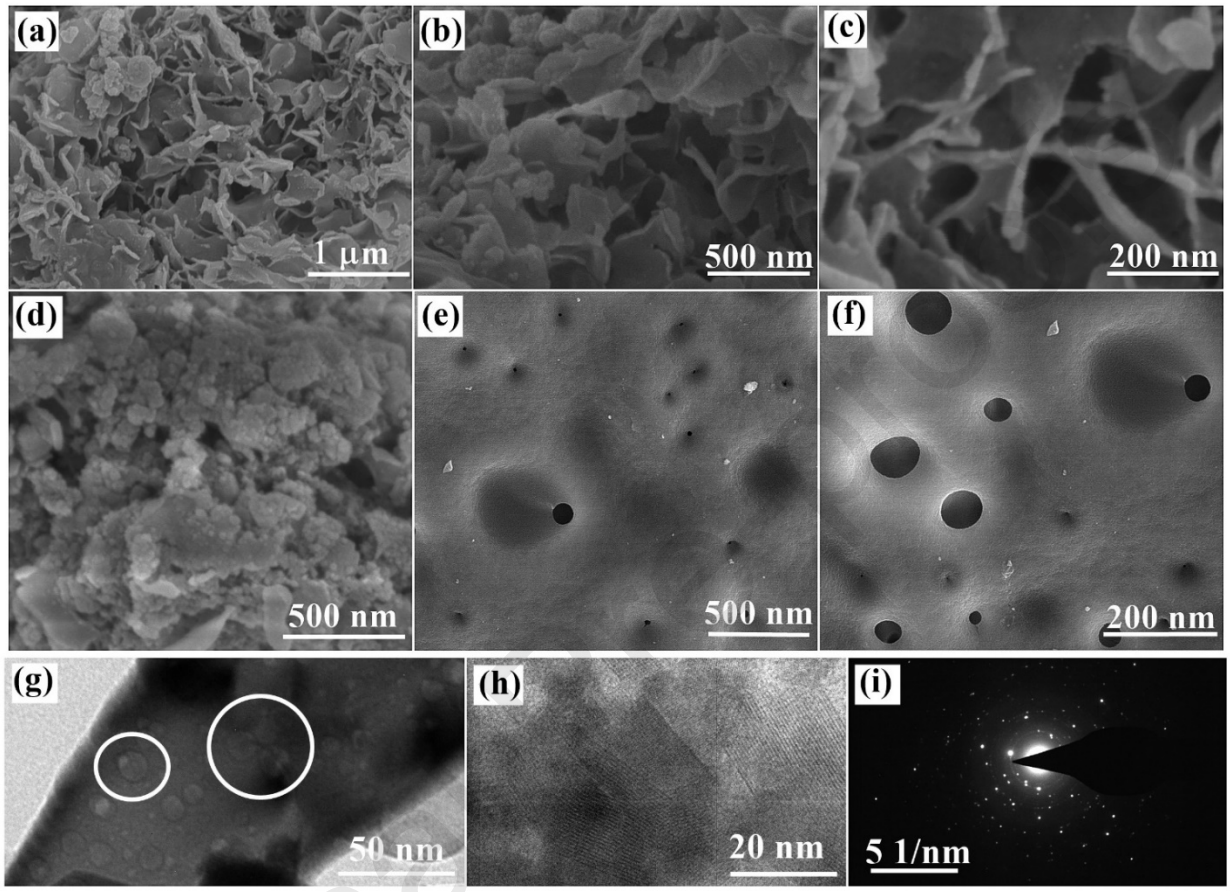

Figure 3. SEM images of (a-c) Zn/Fe LDH; (d) Zn/Fe mixed oxides; (e, f) porous Zn/Fe LDH; and (g-i) TEM images of porous Zn/Fe LDH

XPS analysis was used for the determination of the valence states and chemical composition of the porous Zn/Fe LDH. Complete XPS survey scan of porous Zn/Fe LDH indicates the presence of predominant elements, i.e. Fe, Zn, and O as shown in Figure 4 (a). Deconvolution study of high-resolution XPS spectrum of the elements aided for distinguishing the specific chemical species present in the synthesized adsorbent. The high-resolution Fe2p spectrum reveals the presence of 2 spin-orbit doublets as shown in Figure 4(b). The first doublet was obtained at 716.12 and 730.36 eV that could be related to the presence of Fe^{3+} units in the porous Zn/Fe LDH. The other doublet was present at 710.74 and 724.16 eV attributing the presence of Fe^{2+} moieties [40]. For Zn2p, two

peaks were observed at 1021.73 and 1044.81eV that corresponded to the Zn2p3/2 and Zn2p1/2, respectively [41]. For the deconvoluted spectrum of O1s, two peaks occurred at 530.41 and 532.07eV that marked the presence of Zn-O and Fe-O species in the synthesized adsorbent [35]. Table S1 given in Supplementary data provide the information related to the peak position and their corresponding full width at half maxima (FWHM) of Fe2p, Zn2p, and O1s.

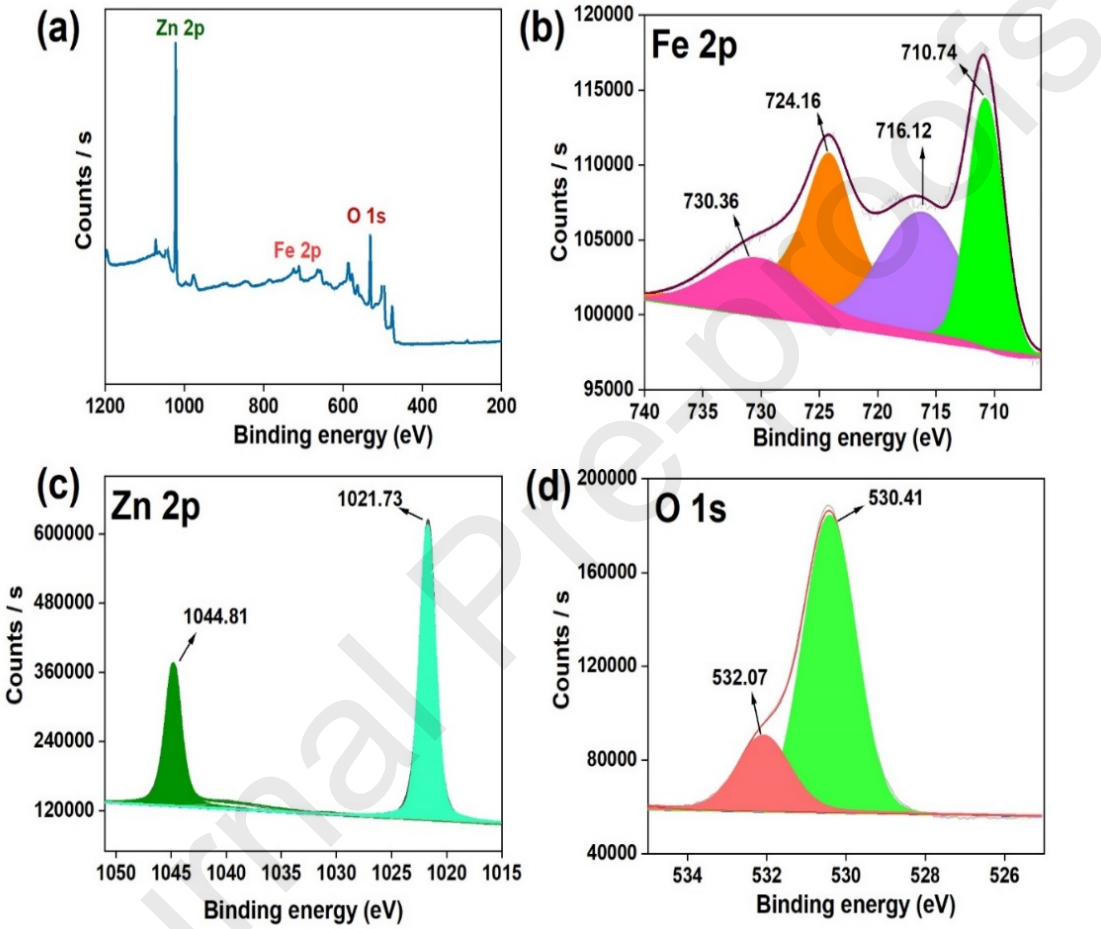

Figure 4. (a) XPS spectrum of porous Zn/Fe LDH; Deconvoluted XPS spectrum of (b) Fe 2p; (c) Zn 2p; and (d) O 1s

N_2 adsorption–desorption isotherms reveal the porosity of the sample. These isotherms can be employed for obtaining the specific surface area and pore size distributions. Figure 5(a, b) represents these isotherms for the Zn/Fe LDH and porous Zn/Fe LDH. Hysteresis loops can be perceived in the 2 isotherms, and these loops exhibited the typical characteristics of type- IV isotherm. Thus, the synthesized LDHs exhibited mesoporous nature. The surface properties related to the surface area, pore-volume, and pore size of the synthesized materials results are summarized

in Table 1. The surface area of Zn/Fe LDH as obtained was 108.863 m^2/g. After the decomposition of intercalated H_2O_2, the surface area got increased to 168.923 m^2/g. The introduction of pores had probably increased the surface area. The average pore size was also increased from 1.66 nm to 6.08 nm. Both samples possess pores with different sizes and high surface area. Thus, Zn/Fe LDH and porous Zn/Fe LDH showed hierarchical pore arrangement, which aid in efficient adsorption of pollutants.

The magnetic properties of the adsorbent help in its easy separation from the mixture after the adsorption experiment. The VSM study was carried out for understanding the magnetic nature of the synthesized adsorbent. The hysteresis loop of porous Zn/Fe LDH exhibited the ferromagnetic character. The coercivity was found to be 534.88Oe and the retentively was 0.129emu/g. The saturation magnetization was 0.668emu/g. The hysteresis loop obtained is presented in Figure 5(c).

Table 1. N_2 adsorption-desorption isotherm parameters

	Surface area (m^2/g)	**Pore volume (cm^3/g)**	**Pore size (nm)**
Zn/Fe LDH	108.863	0.01139	1.66
porous Zn/Fe LDH	168.923	0.09626	6.08

3.3 Adsorption study

Initially, the adsorption performance of Zn/Fe LDH and porous Zn/Fe LDH was conducted for 30 minutes for validating the better activity out of the two (Figure 5(d)). The adsorption rate for Zn/Fe LDH and porous Zn/Fe LDH was calculated to be 60.50 mg/g and 132.67 mg/g (which is nearly 2.19 times greater) within 30 minutes that indicated the high adsorption ability of porous Zn/Fe LDH for CIP exclusion as compared to Zn/Fe LDH. This significant improvement could probably be due to the porous nature and high surface area of porous Zn/Fe LDH. Parameter optimization, isotherm, and kinetic studies were thereafter conducted using porous Zn/Fe LDH.

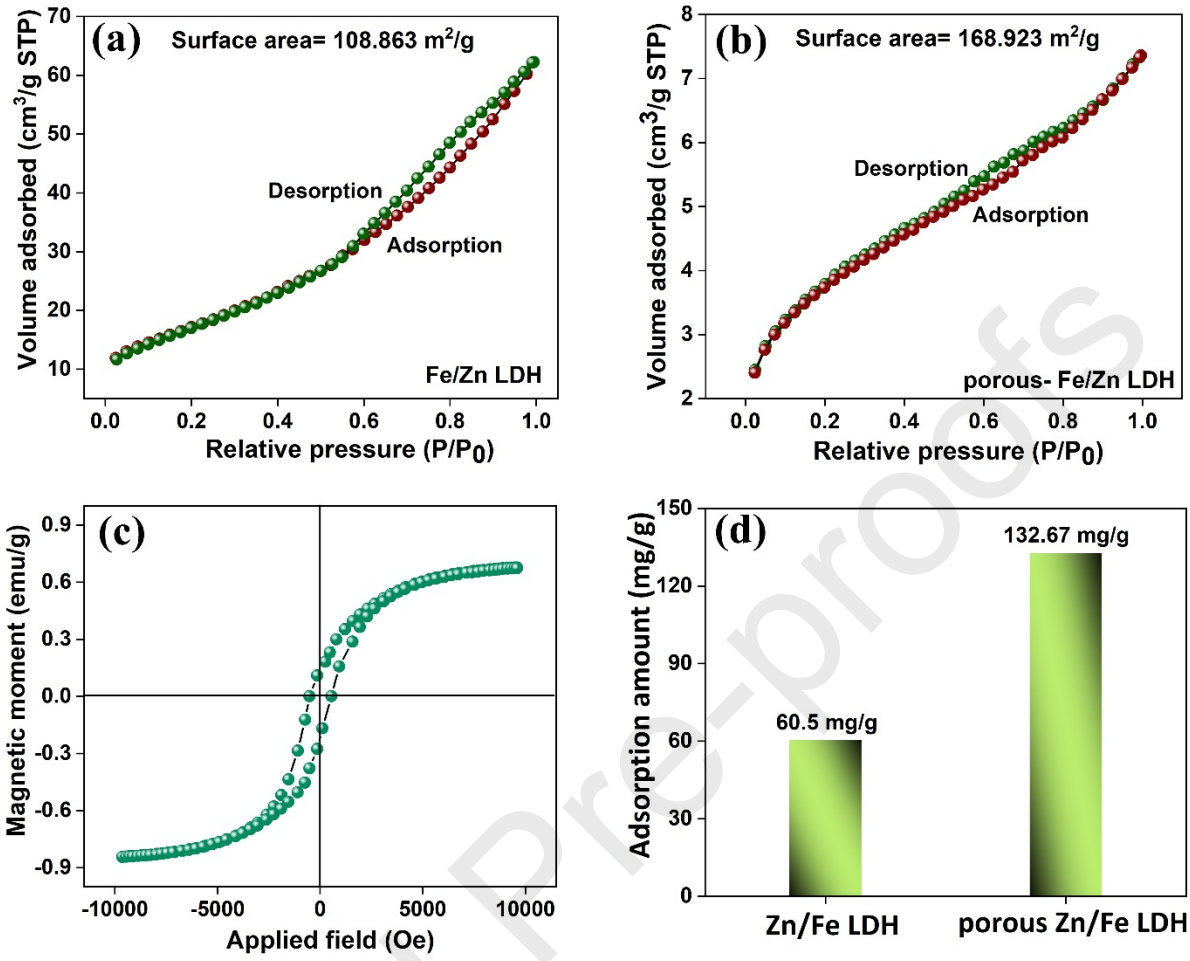

Figure 5. N_2 adsorption- desorption isotherm of (a) Zn/Fe LDH, and (b) porous Zn/Fe LDH; (c) VSM of porous Zn/Fe LDH; (d) Comparison of adsorption of Zn/Fe LDH, and porous Zn/Fe LDH

3.3.1 Effect of adsorbent dose

The adsorbent dose is a significant parameter that influences the adsorption process. The total availability of active sites is generalized from the adsorbent dose. The effect of the adsorbent dose on the adsorption of CIP by porous Zn/Fe LDH was studied by increasing the dosage of the adsorbent from 10 to 40mg, and the results are presented in Figure 6 (a). A general trend was observed in which the adsorption rate first increased to a certain limit and afterward attained a constant value. The initial increase in adsorption rate can be attributed to the increase in the concentration of active adsorption sites. However, after the 15mg adsorbent dose, the increase didn't affect the adsorption rate since the maximum adsorption occurred for that particular

concentration of adsorbate at 15mg. Any further increase in dose only increased the density of the adsorbent in the solution. Thus, 15mg dose of porous Zn/Fe LDH was used for the subsequent adsorption experiments.

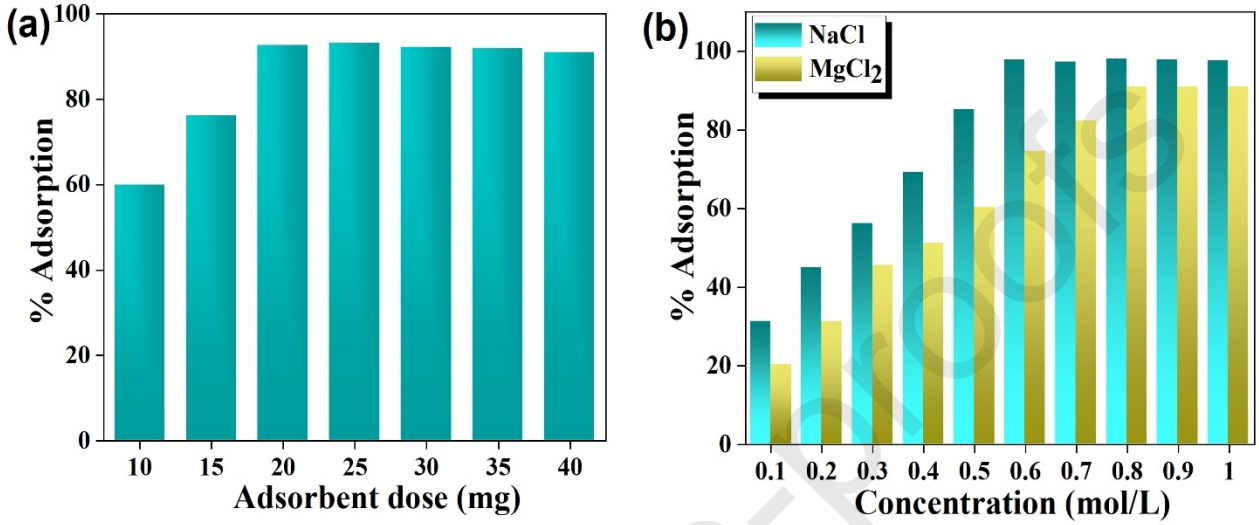

Figure 6. (a) Effect of adsorbent dose (Reaction conditions: Solution volume= 50 mL, CIP concentration= 50 mg/L, and Time= 180 minutes); and (b) Effect of ionic strength (Reaction conditions: Adsorbent dose= 20 mg, Solution volume= 50 mL, CIP concentration= 50 mg/L, and Time= 180 minutes)

3.3.2 Effect of ionic strength

Considering the wastewater conditions, the presence of salts is quite common and their presence can significantly affect the adsorption rate. For determining the effect of ionic strength on the adsorption efficiency of porous Zn/Fe LDH for CIP, 2 different salts, NaCl, and $MgCl_2$, were used. Solutions of different salt concentrations were prepared in the range of 0.1 to 1.0 mol/L that were mixed with 15 mg of adsorbent and 50 mg/L CIP concentration. The results obtained are presented in Figure 6 (b) and they exhibited that the adsorption rate was significantly improved in the presence of salts. In case of NaCl, the adsorption rate first increased from 0.1 to 0.6 mol/L and thereafter, became constant. Probable reason for this could be the salting out effect between CIP molecules and NaCl that resulted in decreased solubility of CIP molecules in the aqueous solution [42, 43]. This decreased solubility facilitated the diffusion of more CIP molecules to the surface of porous Zn/Fe LDH which resulted in the increased adsorption rate. Same trend was observed in

case $MgCl_2$, however, the equilibrium concentration was found to be 0.8 mol/L. In addition, the adsorption rate was more prominent in case of NaCl as compared to the $MgCl_2$ since the dissociation of NaCl in water is easier than that of $MgCl_2$.

3.3.3 Effect of pH

The solution pH affects the surface properties of adsorbent as well as adsorbate which in turn affects the adsorption rate. The adsorption of CIP in different solution pH in the range of 3- 10 was studied and is presented in Figure 7 (a). CIP adsorption onto porous Zn/Fe LDH was found to be highly dependent on the solution pH. The adsorption rate increased with an increase in pH from 4 to 6.5 and afterward decreased indicating that extremely acidic and basic conditions decreased the CIP adsorption.

The exact mechanism for the variation in adsorption rate can be linked to the variation in the surface properties that occurred in different pH solutions and the point of zero charge (PZC) effectively explains that. In the present study, the PZC of porous Zn/Fe LDH is 7.18 as shown in Figure 7 (b) indicating the positively charged surface below 7.18 and negatively charged surface above 7.18. The surface charge of porous Zn/Fe LDH originated from the adsorption of different ions present in the solution as:

Below 7.18 $LDH - OH + H_3O^+ \rightarrow LDH - OH_2{}^+ + H_2O$ (3)

Above 7.18 $LDH - OH + OH^- \rightarrow LDH - O^- + H_2O$ (4)

Protonation and deprotonation processes make the surface of porous Zn/Fe LDH positively and negatively charged. Besides, the ion exchange mechanism resulting from the exchange between intercalated anions with the hydroxyl radicals could also make the surface of porous Zn/Fe LDH negatively charged [44]. In addition to porous Zn/Fe LDH, CIP also shows different behavior in different pH solutions as shown in Figure 7 (c). It exists as CIP^+ at pH < 5.9 due to the protonation of the secondary amine on the piperazine group. It exists in the zwitterionic state between pH 6.1 and 8.9 due to the presence of balanced charge between the deprotonated carboxylic acid group and protonated secondary amine on the piperazine group. However, as the solution pH is increased above > 8.9, the deprotonation of the secondary amine on the piperazine group generates the anionic form, CIP^-. As presented in Figure 7 (a), the working pH for CIP adsorption onto porous

Zn/Fe LDH is 6.5 which is indicative of the electrostatic interactions between the negatively charged CIP molecules and positively charged porous Zn/Fe LDH surface. Low adsorption rate < 5.9 and > 8.9 pH can be due to the electrostatic repulsive forces between the CIP species and porous Zn/Fe LDH surface. Thus, electrostatic interactions between CIP molecules and porous Zn/Fe LDH was one of the chief factors affecting the adsorption.

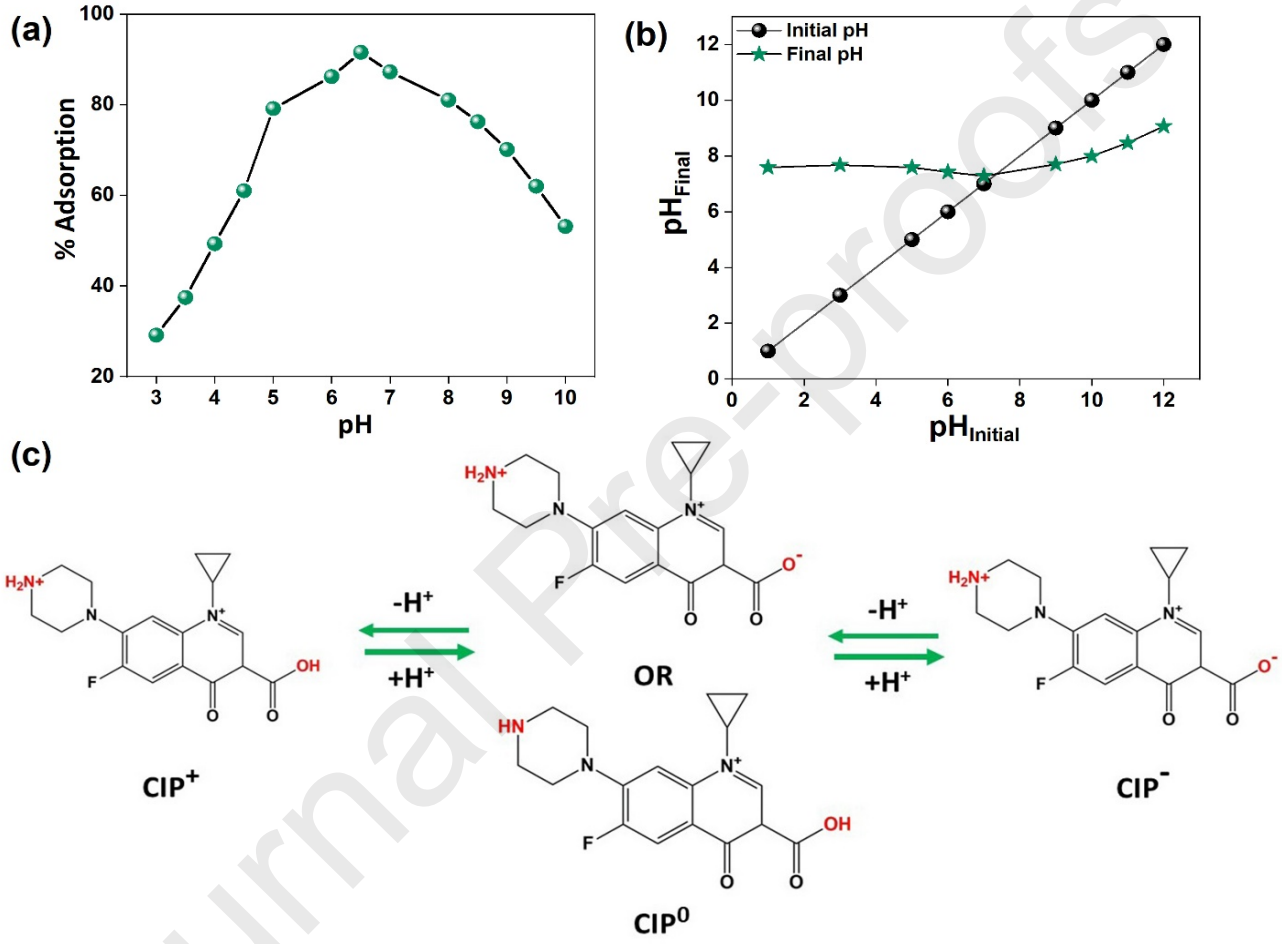

Figure 7 (a). Effect of solution pH on the adsorption rate; (b) Point of zero charge of porous Zn/Fe LDH; and (c) Structural changes of CIP in different pH (Reaction conditions: Adsorbent dose= 20 mg, Solution volume= 50 mL, CIP concentration= 50 mg/L, and Time= 180 minutes)

3.4 Adsorption isotherms

Adsorption isotherm analysis is an effective way for determining the interactions between the adsorbent and adsorbate molecules [45]. Before analyzing the isotherms models, variation in

adsorption amount w.r.t initial concentration of CIP solution at different temperatures was studied and is presented in Figure 8 (a). At a particular temperature, an increase in the solution concentration increases the adsorption amount and ultimately acquires equilibrium or saturation point. With the increase in temperature, the maximum adsorption amount decreased considerably indicating the negative effect of temperature on the adsorption amount. This indicated that the undertaken adsorption experiment can be exothermic. For further formulating the mechanism of adsorption, two isotherm models, namely, Langmuir and Freundlich are employed and their details are presented in Supplementary file as Text S5 [46, 47].

Comparison of fitting curves using the correlation coefficient value (R^2) shows that the fitting curves of the Freundlich model fit the adsorption data more perfectly than that of Langmuir model, as shown in Figure 8 (b, c) and Table 2. At different temperature conditions, R^2 values are greater than 0.99, indicating that the better tendency of the Freundlich model in explaining the undertaken adsorption data. Maximum adsorption capacity as determined from the Langmuir model is 344.83 mg/g at 298 K. The Langmuir constant, K_L specifies the extent of binding interactions between the adsorbent and adsorbate[48, 49]. Maximum was obtained at 298 K specifying maximum interactions at this temperature. The desired value of 1/n is obtained (<1) indicating the favorable adsorption. The high adsorption capacity of porous Zn/Fe LDH can be linked to its porous structure and also to the high surface area. Also, some of the CIP molecules may get intercalated into the basal spacing indicating multiple possibilities for the obtained high adsorption capacity. Also, a comparison Table 3 is presented that indicated the superior adsorption capacity of porous Zn/Fe LDH as compared to other adsorbents reported in the literature.

In addition, the influence of temperature can also be clearly observed on the adsorption rate. The maximum adsorption capacity (qm) decrease with the increase in temperature from 298 to 318 K. This indicated that the temperature adversely affected the adsorption process. The rise in temperature may had decreased the penetration of CIP molecules across the surface or inside the pores of the adsorbent. Also, the rise may had increased the mobility of CIP molecules to such as great extent that ultimately decreased the chances of interactions with the porous Zn/Fe LDH surface. The temperature influence was further justified by the thermodynamic study as presented in Section 3.6.

Table 2. Adsorption isotherm parameters

Langmuir	Temperature (K)	qm (mg/g)	K_L (L/mg)	R^2
	298	344.83	0.021	0.982
	308	227.27	0.019	0.965
	318	212.76	0.014	0.942
Freundlich	**Temperature (K)**	**1/n**	**K_F (L/mg)**	**R^2**
	298	0.868	5.688	0.998
	308	0.732	6.765	0.993
	318	0.748	6.547	0.991

Table 3. Comparison of CIP adsorption onto various adsorbents

Adsorbent	Absorbent dose (mg)	Time (hrs)	Solution pH	qm (mg/g)	Reference
Surface-modified carbon	2.5	72	5	300	[50]
Sodium alginate GO	15	18	4	86.12	[51]
Magnetic biochar	50	12	6	68.9	[52]
Zinc-benzenedicarboxylate (MOF-5)	50	9	5.5	98.2	[53]
Graphitic ordered mesoporous carbon	30	24	6	267.4	[54]
Copper-glutamate MOF	50	2	4	61.35	[55]
Nitrilotriacetic acid-functionalized magnetic graphene oxide nanocomposite	10	14	9	282.06	[56]
3D porous graphene hydrogel	25	120	6	237.5	[57]

$CoFe_2O_4$/Activated carbon@Chitosan	10	-	5	188.68	[58]
Fe_3O_4/GO/citrus peel-derived magnetic bio-nanocomposite	20	36	6	283.44	[59]
porous Zn/Fe LDH	20	10	6.5	344.83	**This study**

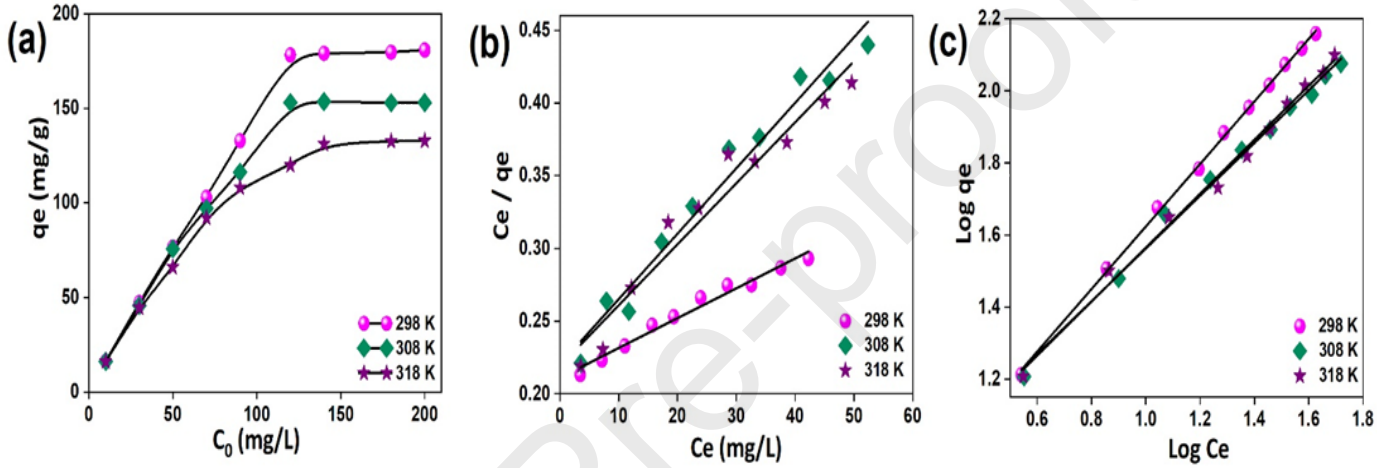

Figure 8. (a) Variation in adsorption amount w.r.t initial concentration at different temperatures; and Adsorption isotherm models (b) Langmuir model and (c) Freundlich (Reaction conditions: Adsorbent dose= 20 mg, Solution volume= 50 mL, pH= 6.5, Time= 10 hours)

3.5 Adsorption kinetics

Adsorption kinetics can be described as a plot that explains the rate of adsorption of adsorbate molecules onto the surface of solid-phase adsorbent at a given adsorbent dose, pH, and temperature. It helps in determining the rate of undertaken adsorption process [60]. Herein, 4 different kinetic models, namely pseudo-first-order, pseudo-second-order, Intraparticle diffusion, and Elovich were employed for determining whether the undertaken adsorption inclined towards the chemisorption or physisorption and the exact mechanism of adsorption. The details of each model used are presented in the supplementary file as Text S6 [61].

The contact time between adsorbate and adsorbent influences the rate of adsorption to a great extent. It increases the chances of interactions between the two systems. In the present study, the

maximum time required for achieving the equilibrium point was 180 minutes as presented in Figure 9 (a). It can be linked with the presence of numerous vacant active sites on the adsorbent surface during the initial 180 minutes that could be used for adsorption. However, with time, the active sites become less available for adsorption due to repulsive forces between the surface adsorbed molecules and free molecules in the solution. As a result, the adsorption rate was decreased and ultimately attained equilibrium after 180 minutes.

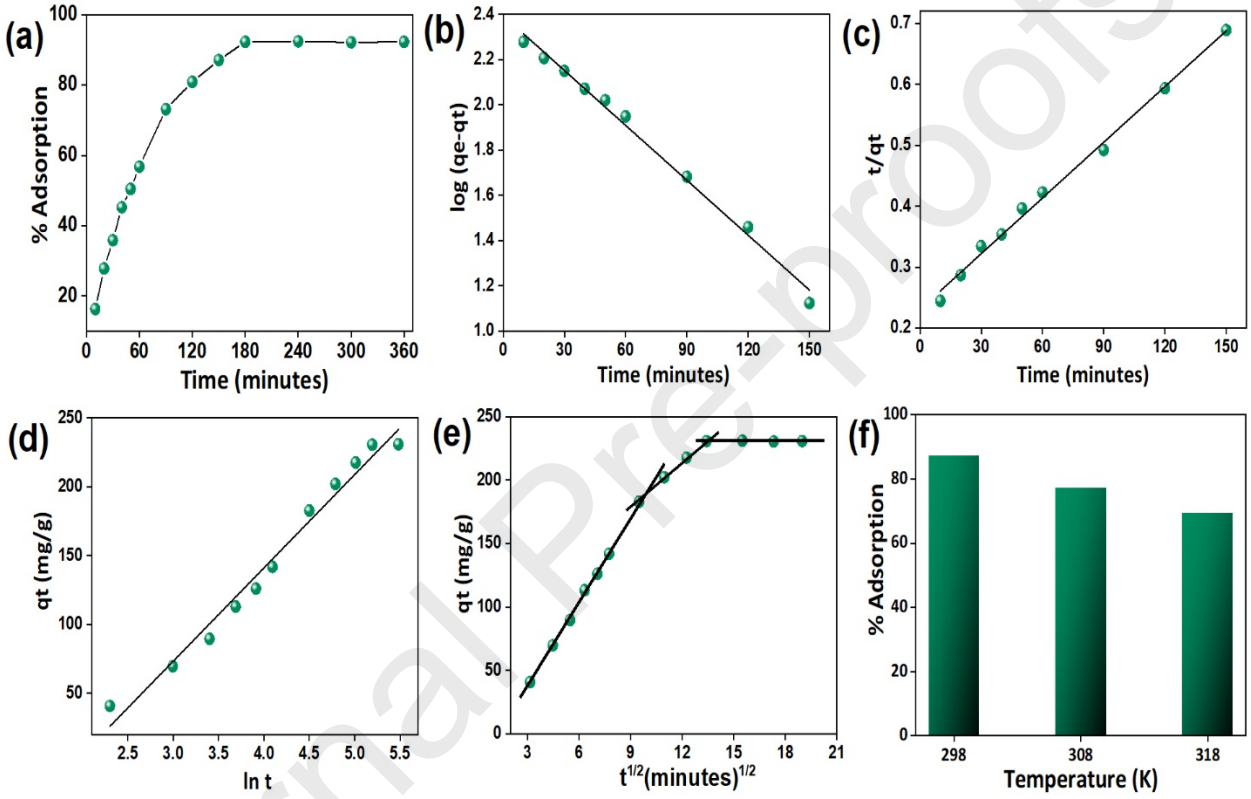

Figure 9. (a) Percent adsorption trend w.r.t. change in contact time; (b) Pseudo- first order; (c) Pseudo- second order; (d) Elovich model; (e) Intraparticle diffusion model, (Reaction conditions: CIP concentration= 50 mg/L, Time= 360 minutes, pH= 6.5, rpm= 100 and temperature=298K) and (f) Percent adsorption trend w.r.t change in temperature (Reaction conditions: CIP concentration= 50 mg/L, Time= 360 minutes, pH= 6.5, and rpm= 100)

The results of 4 kinetic models are presented in Figure 9 (b-e). The applicability of the kinetic model was generalized on the basis of high R^2 values obtained using the linear plot for pseudo-first-order and pseudo-second-order and the comparison of qe values (experimental and calculated). The values presented in Table 4 specifies the better applicability of pseudo-second-

order model in elucidating the adsorption of CIP molecules onto porous Zn/Fe LDH indicating the interactions were mainly governed by chemisorption [62]. In fact, the major adsorption mechanisms between CIP molecules and porous Zn/Fe LDH was dominated Cπ- metal bonding, and anion exchange. Also, the comparison of the rate constants (k_1 ad k_2) favored the pseudo-second-order model more. The chemical behavior of undertaken adsorption process was further elaborated using Elovich kinetic model. The initial adsorption rate as determined was found to be 10.068 mg/g.min that well relates to the kinetic data and the probable reason for the equilibrium attainment at 180 minutes. Also, the value of activation energy, β is 0.0147 which is quite low indicating quite an effective adsorption.

Further, the intraprticle diffusion model was employed for determining the step- reaction mechanism. The graph presented in Figure 9 (e) shows that the adsorption followed a 3- step mechanism. The value of C as determined from the linear plot of $t_{1/2}$ vs q_t is 33.546 which is non-zero signifying the intraparticle diffusion was not the only rate-limiting step, however, several complex mechanisms were undergoing.

Table 4. Adsorption kinetic parameters

Pseudo- first order	**q_e exp (mg/g)**	**q_e cal (mg/g)**	**k_1 (min^{-1})**	**R^2**
	230.988	248.31	0.0184	0.991
Pseudo- second order		**q_e cal (mg/g)**	**k_2 (g/mg.min)**	**R^2**
		243.90	0.0007	0.993
Intraparticle diffusion		**C**	**K_{id} (mg/g.min)**	**R^2**
		33.546	12.642	0.855
Elovich		**α (mg/g.min)**	**β (g/mg)**	**R^2**
		10.068	0.0147	0.978

3.6 Effect of temperature and Thermodynamic study

The effect of temperature on the adsorption of CIP was also studied in detail. The adsorption studies were carried out at 3 different temperatures, viz., 298, 308, and 318 K and the results are shown in Figure 9 (f). In the present study, the increase in solution temperature decreased the adsorption rate and maximum adsorption rate was obtained at 298 K. Rise in temperature increases the kinetic energy of the molecules, as a result of which the chances to the interactions between adsorbate and adsorbent decreases. These results are even consistent with the isotherm study in which maximum adsorption capacity was obtained at 298 K and it got decreased as the temperature was increased.

For discovering the thermodynamic characteristics of the undertaken adsorption experiment, the adsorption equilibrium reactions were carried out as a function of temperature. The thermodynamic parameters associated with the adsorption process were determined from the adsorption isotherms at 3 different temperatures; viz. 298, 308, and 318 K. Different thermodynamic parameters; ΔG^0, ΔH^0, and ΔS^0 were determined using the following equations [63]:

$$k_C = \frac{q_e}{C_e} \tag{11}$$

$$\Delta G^0 = -RTlnk_C \tag{12}$$

$$lnk_C = -\frac{\Delta H^0}{RT} + \frac{\Delta S^0}{R} \tag{13}$$

Where ΔG^0 was determined from equation 12 and ΔH^0 and ΔS^0 were determined from the slope and intercept by the linear plot of ln k_C versus 1/T(1/K) [64]. The linear plot of thermodynamic study for the adsorption of CIP onto porous Zn/Fe LDH was determined and values for various parameters are presented in Table 5. The negative value of ΔH^0 denotes the exothermic nature of the adsorption interactions and the positive value of ΔS^0 specifies the increased randomness at the interface of solid-liquid mediums. All the ΔG^0 values are negative, suggesting the adsorption of CIP on porous Zn/Fe LDH was spontaneous and thermodynamically favorable.

Table 5. Thermodynamic parameters

Temperature (K)	ΔG^0 (KJ/mol)	ΔH^0 (KJ/mol)	ΔS^0 (J/molK)
298	-3.361	-8.513	17.254
308	-3.234		
318	-3.014		

3.7 Adsorption mechanism

The adsorption capacity of porous Zn/Fe LDH was found to be quite appreciable for CIP as generalized by the above presented studies. A probable scheme showing the CIP adsorption onto porous Zn/Fe LDH is shown in Figure 10. The Zn/Fe LDH was converted into Zn/Fe mixed oxide along with the removal of interlayer molecules by the calcination treatment. Using the "memory effect", the Zn/Fe mixed oxide was able to regenerate its original layered structure when placed in the H_2O_2 environment which was successfully converted to porous structure by the thermal treatment. When the synthesized porous Zn/Fe LDH was placed in CIP aqueous solution, various interactions occurred. The high surface area and porous nature of the synthesized adsorbent could have resulted in the surface and pore diffusion of CIP molecules.

Due to the anion exchange ability of the LDHs, some of the CIP molecules may acquire the intercalated position [65]. The intercalation of CIP was further ascertained by the XRD results carried out after the adsorption experiments and the results are presented in the Supplementary Data Figure S2. The results indicated that the prominent peaks of the porous Zn/Fe LDH were obtained as such. But the basal spacing got increased from 8.61Å to 10.56 Å after the CIP adsorption. The increase in basal spacing is an indication of the successful intercalation of CIP molecules in the interlayer of porous Zn/Fe LDH.

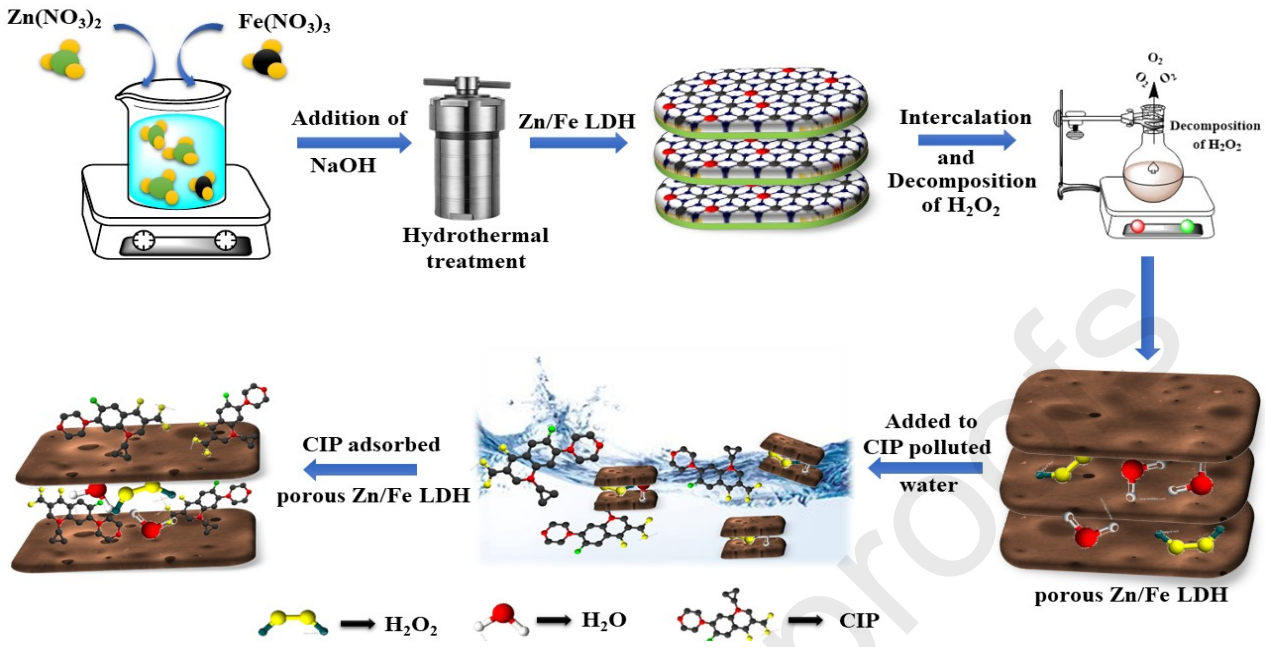

Figure 10. Schematic mechanism of adsorption of CIP molecules onto porous Zn/Fe LDH

The chances of surface adsorption were also probable in which the H- bonding, and metal- Cπ bonding may played a significant role. The -NH- groups from the CIP molecules and hydroxyl groups from porous Zn/Fe LDH resulted in the formation of hydrogen bonds (h-bonds) between them. Other interactions possible were metal-Cπ interactions which are basically the electrostatic interactions in which the positively charged cations interacts with a negatively charged electron cloud of π- systems [66]. Herein, iron and zinc showed these interactions with the π- electron cloud of CIP molecules.

Furthermore, XPS was employed to study the elemental composition and their chemical state. The complete spectrum of CIP adsorbed porous Zn/Fe LDH is presented in Supplementary file as Figure S3 that shows the presence of C, F, O, N, Fe, and Zn indicating the presence of desired elements in the synthesized adsorbent. For C 1s, prominent peaks were observed at 285.17, 286.41, and 286.64 eV respectively that correspond to the C-N, C-OH, and C=O, respectively (Figure 11(a)) [67-69]. These groups are characteristic of CIP indicating its presence in the recovered sample. For N 1s, three peaks appeared at 399.14, 399.66, and 400.80 eV. The N-C and N-O bonds were ascertained by the appearance of peaks at 399.14, and 399.66 eV, respectively [70]. The peak at 400.80 eV corresponded to the C-N-O bond formed between the C-N group of CIP and M-O of LDH. For F 1s, peaks were observed at 684.65 and 687.38 eV that marked the presence of –F unit

in the analyzed sample which is characteristic of CIP molecules [70]. The O 1s spectrum shows the major peaks at 529.96, 531.23, and 532.13 eV. After CIP adsorption, a new emerged at 529.96 eV that can be linked to the C=O bond for the adsorbed CIP molecules [71, 72]. The other peaks were for the M-O bonds as explained before in Section 3.2. For Zn 2p and Fe 2p, a slight shift in the binding energy was observed after CIP adsorption that suggested the formation of a complex, CIP- porous Zn/Fe LDH.

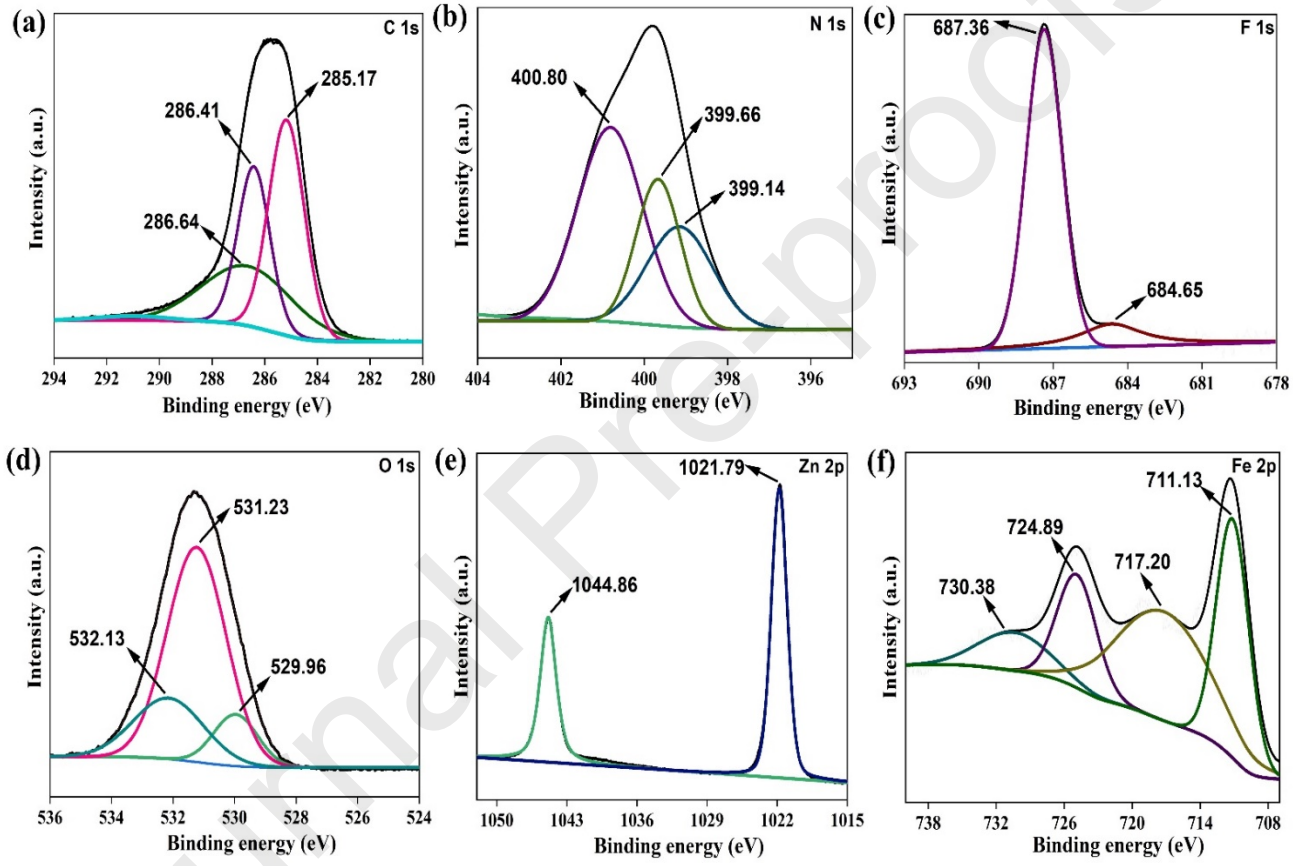

Figure 11. After adsorption of CIP onto porous Zn/Fe LDH (a-f) XPS spectra

3.8 Study of adsorption of other pollutants

In addition, we studied the adsorption capacity of porous Zn/Fe LDH for other pollutants too, such as, malachite green (MG) dye, methylene blue (MB), and tetracycline (TC). A general properties or specifications of the 3 pollutants are presented in Supplementary file as Table S2. Individual and comparative studies were carried out for generalizing the adsorption performance of porous Zn/Fe LDH. Figure 12 (a) shows that appreciable MG, MB, and TC adsorption rate was obtained

during the individual experiments. However, in the comparative study (Figure 12 (b)), the adsorption rate was comparatively decreased that can probably be due to the competitive adsorption between the three, but it still maintained quite an appreciable rate that generalized the adsorption proficiency of porous Zn/Fe LDH.

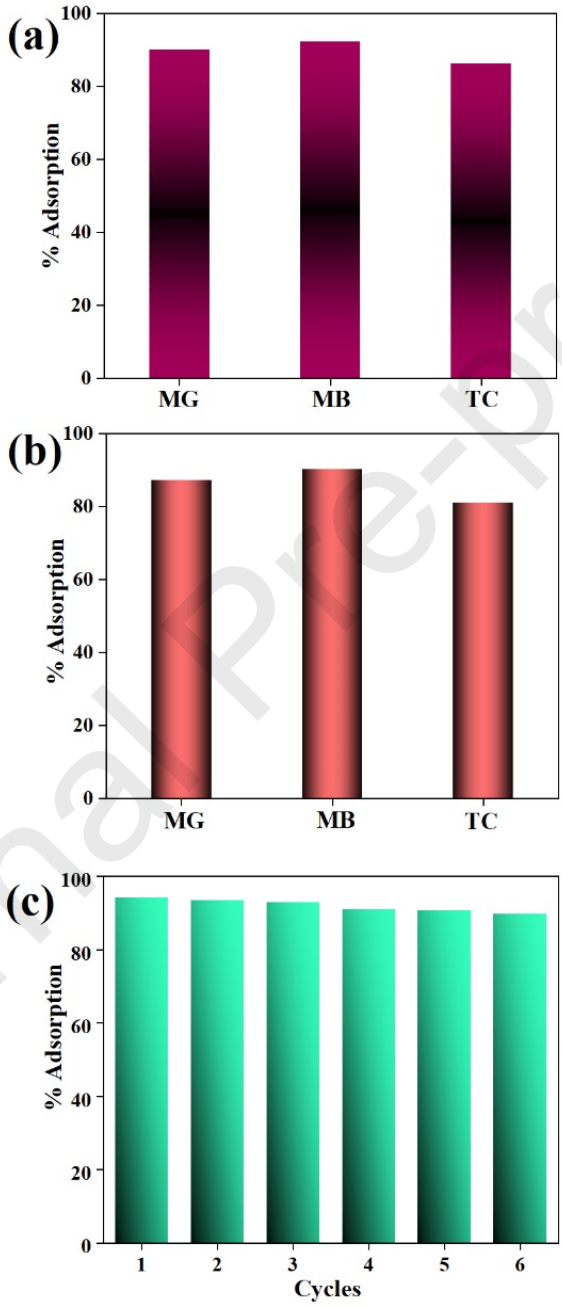

Figure 12. Adsorption of MG, MB and TC onto porous Zn/Fe LDH (a) Individual; and (b) Comparative and (c) Reusability study of porous Zn/Fe LDH for 6 consecutive cycles

3.9 Reusability study

After adsorption, the desorption and reusability experiments were carried out. The desorption experiments of porous Zn/Fe LDH were carried out in 0.1M HCl solution multiple times. The alternative adsorption and desorption experiments were carried out for 6 cycles and the results are provided in Figure 12 (c). After 6 cycles, only a small decrease in adsorption rate was observed indicative of the high adsorption ability and stability of porous Zn/Fe LDH. This lead to the generalization about the practical applicability of the synthesized porous Zn/Fe LDH as an adsorbent. Therefore, it can also be applied for the adsorption of other adsorbates too.

4. Conclusions

In summary, we fabricated a novel porous Zn/Fe LDH by the decomposition of H_2O_2 in the interlayer system. The complete synthesis mechanism of LDH was explained in context to the Zeta potential variation and a proper step-wise synthesis mechanism was proposed. The characterizations were successfully carried out and XRD, BET, and SEM provided many useful elucidations. The synthesized porous Zn/Fe LDH exhibited excellent adsorption proficiency towards CIP removal from the aqueous solution. According to the Langmuir isotherm, the maximum adsorption capacity was 344.83 mg/g at 298 K. The underlying adsorption kinetic studies revealed the better applicability of pseudo- second order model in the explaining the CIP adsorption onto porous Zn/Fe LDH. The thermodynamic study generalized the spontaneous and exothermic nature of the undertaken experiment. Besides, the synthesized adsorbent was found to exhibit high reusability. The highly enhanced adsorption activity of the porous Zn/Fe LDH could be attributed to the high surface area, unique morphology, and porous nature.

Acknowledgement

This work was supported by the Distinguished Scientist Fellowship Program (DSFP) at King Saud University, Riyadh, Saudi Arabia.

References

[1] X. Li, S. Chen, X. Fan, X. Quan, F. Tan, Y. Zhang, J. Gao, Adsorption of ciprofloxacin, bisphenol and 2-chlorophenol on electrospun carbon nanofibers: in comparison with powder activated carbon, Journal of colloid and interface science, 447 (2015) 120-127.
[2] L. Yao, H. Yang, Z. Chen, M. Qiu, B. Hu, X. Wang, Bismuth oxychloride-based materials for the removal of organic pollutants in wastewater, Chemosphere, (2020) 128576.

[3] K. Gupta, J.-B. Huo, J.-C.E. Yang, M.-L. Fu, B. Yuan, Z. Chen, $(MoS_4)^{2-}$ intercalated $CAMoS_4$·LDH material for the efficient and facile sequestration of antibiotics from aqueous solution, Chemical Engineering Journal, 355 (2019) 637-649.
[4] X. Liu, R. Ma, L. Zhuang, B. Hu, J. Chen, X. Liu, X. Wang, Recent developments of doped g-C3N4 photocatalysts for the degradation of organic pollutants, Critical Reviews in Environmental Science and Technology, 51 (2021) 751-790.
[5] G. Sharma, A. Kumar, S. Sharma, A.a.H. Al-Muhtaseb, M. Naushad, A.A. Ghfar, T. Ahamad, F.J. Stadler, Fabrication and characterization of novel Fe0@Guar gum-crosslinked-soya lecithin nanocomposite hydrogel for photocatalytic degradation of methyl violet dye, Separation and Purification Technology, 211 (2019) 895-908.
[6] Y. Sun, H. Li, G. Li, B. Gao, Q. Yue, X. Li, Characterization and ciprofloxacin adsorption properties of activated carbons prepared from biomass wastes by H_3PO_4 activation, Bioresource technology, 217 (2016) 239-244.
[7] C. Liang, X. Zhang, P. Feng, H. Chai, Y. Huang, ZIF-67 derived hollow cobalt sulfide as superior adsorbent for effective adsorption removal of ciprofloxacin antibiotics, Chemical engineering journal, 344 (2018) 95-104.
[8] C. Wang, J. Kim, J. Tang, J. Na, Y.M. Kang, M. Kim, H. Lim, Y. Bando, J. Li, Y. Yamauchi, Large-scale synthesis of MOF-derived superporous carbon aerogels with extraordinary adsorption capacity for organic solvents, Angewandte Chemie, 132 (2020) 2082-2086.
[9] M. Hao, M. Qiu, H. Yang, B. Hu, X. Wang, Recent advances on preparation and environmental applications of MOF-derived carbons in catalysis, Science of the Total Environment, (2020) 143333.
[10] A. Mudhoo, D. Mohan, C.U. Pittman, G. Sharma, M. Sillanpää, Adsorbents for real-scale water remediation: Gaps and the road forward, Journal of Environmental Chemical Engineering, 9 (2021) 105380.
[11] J. Chen, J. Feng, W. Yan, Influence of metal oxides on the adsorption characteristics of PPy/metal oxides for Methylene Blue, Journal of colloid and interface science, 475 (2016) 26-35.
[12] P.B. Vilela, C.A. Matias, A. Dalalibera, V.A. Becegato, A.T. Paulino, Polyacrylic acid-based and chitosan-based hydrogels for adsorption of cadmium: Equilibrium isotherm, kinetic and thermodynamic studies, Journal of Environmental Chemical Engineering, 7 (2019) 103327.
[13] Z. Huang, Y. Li, W. Chen, J. Shi, N. Zhang, X. Wang, Z. Li, L. Gao, Y. Zhang, Modified bentonite adsorption of organic pollutants of dye wastewater, Materials Chemistry and Physics, 202 (2017) 266-276.
[14] S.F. Lütke, A.V. Igansi, L. Pegoraro, G.L. Dotto, L.A. Pinto, T.R. Cadaval Jr, Preparation of activated carbon from black wattle bark waste and its application for phenol adsorption, Journal of Environmental Chemical Engineering, 7 (2019) 103396.
[15] X. Liu, H. Pang, X. Liu, Q. Li, N. Zhang, L. Mao, M. Qiu, B. Hu, H. Yang, X. Wang, Orderly porous covalent organic frameworks-based materials: superior adsorbents for pollutants removal from aqueous solutions, The Innovation, (2021) 100076.
[16] G. Sharma, S. Sharma, A. Kumar, A.a.H. Al-Muhtaseb, M. Naushad, A.A. Ghfar, G.T. Mola, F.J. Stadler, Guar gum and its composites as potential materials for diverse applications: A review, Carbohydrate Polymers, 199 (2018) 534-545.
[17] O. Moradi, G. Sharma, Emerging novel polymeric adsorbents for removing dyes from wastewater: A comprehensive review and comparison with other adsorbents, Environmental Research, 201 (2021) 111534.

[18] M. Haghighizadeh, K. Zare, H. Aghaie, M. Monajjemi, Preparation and characterization of Chicory leaf powder and its application as a nano-native plant sorbent for removal of Acid Blue 25 from aqueous media: Isotherm, kinetic and thermodynamic study of the adsorption phenomenon, Journal of Nanostructure in Chemistry, 10 (2020) 75-86.
[19] G. Sharma, M. Naushad, D. Pathania, A. Mittal, G.E. El-desoky, Modification of Hibiscus cannabinus fiber by graft copolymerization: application for dye removal, Desalination and Water Treatment, 54 (2015) 3114-3121.
[20] Z.-z. Yang, C. Zhang, G.-m. Zeng, X.-f. Tan, H. Wang, D.-l. Huang, K.-h. Yang, J.-j. Wei, C. Ma, K. Nie, Design and engineering of layered double hydroxide based catalysts for water depollution by advanced oxidation processes: a review, Journal of Materials Chemistry A, 8 (2020) 4141-4173.
[21] G. Di, Z. Zhu, H. Zhang, J. Zhu, H. Lu, W. Zhang, Y. Qiu, L. Zhu, S. Küppers, Simultaneous removal of several pharmaceuticals and arsenic on Zn-Fe mixed metal oxides: combination of photocatalysis and adsorption, Chemical Engineering Journal, 328 (2017) 141-151.
[22] Z. Liu, R. Ma, M. Osada, N. Iyi, Y. Ebina, K. Takada, T. Sasaki, Synthesis, anion exchange, and delamination of Co− Al layered double hydroxide: assembly of the exfoliated nanosheet/polyanion composite films and magneto-optical studies, Journal of the American Chemical Society, 128 (2006) 4872-4880.
[23] G.E.d.S. dos Santos, P.V. dos Santos Lins, L.M.T. de Magalhães Oliveira, E.O. da Silva, I. Anastopoulos, A. Erto, D.A. Giannakoudakis, A.R.F. de Almeida, J.L. da Silva Duarte, L. Meili, Layered double hydroxides/biochar composites as adsorbents for water remediation applications: Recent trends and perspectives, Journal of Cleaner Production, (2020) 124755.
[24] Q. Wang, D. O'Hare, Recent advances in the synthesis and application of layered double hydroxide (LDH) nanosheets, Chemical reviews, 112 (2012) 4124-4155.
[25] C. Fang, X. Zhang, Y. Lei, Y. Yuan, Y. Xiang, Nitrogen removal via core-shell bio-ceramic/Zn-layer double hydroxides synthesized with different composites for domestic wastewater treatment, Journal of Cleaner Production, 181 (2018) 618-630.
[26] M. Bukhtiyarova, A review on effect of synthesis conditions on the formation of layered double hydroxides, Journal of Solid State Chemistry, 269 (2019) 494-506.
[27] G. Mishra, B. Dash, S. Pandey, Layered double hydroxides: A brief review from fundamentals to application as evolving biomaterials, Applied Clay Science, 153 (2018) 172-186.
[28] A. Grover, I. Mohiuddin, A.K. Malik, J.S. Aulakh, K.-H. Kim, Zn-Al layered double hydroxides intercalated with surfactant: Synthesis and applications for efficient removal of organic dyes, Journal of Cleaner Production, 240 (2019) 118090.
[29] F. Cavani, F. Trifiro, A. Vaccari, Hydrotalcite-type anionic clays: Preparation, properties and applications, Catalysis today, 11 (1991) 173-301.
[30] P.G. Rodriguez, M. De Ruiter, T. Wijnands, J.E. ten Elshof, Porous layered double hydroxides synthesized using oxygen generated by decomposition of hydrogen peroxide, Scientific reports, 7 (2017) 1-9.
[31] M.-A. Thyveetil, P.V. Coveney, J.L. Suter, H.C. Greenwell, Emergence of undulations and determination of materials properties in large-scale molecular dynamics simulation of layered double hydroxides, Chemistry of Materials, 19 (2007) 5510-5523.
[32] A. Leão, L. de França, C. de Cunha, F. Marinho, M. Soares, J. Soares-Sobrinho, In-line monitoring of layered double hydroxide synthesis and insights on formation mechanism and kinetics, Applied Clay Science, 179 (2019) 105130.

[33] R. kumar Allada, A. Navrotsky, H.T. Berbeco, W.H. Casey, Thermochemistry and aqueous solubilities of hydrotalcite-like solids, Science, 296 (2002) 721-723.
[34] J.J. De Yoreo, P.G. Vekilov, Principles of crystal nucleation and growth, Reviews in mineralogy and geochemistry, 54 (2003) 57-93.
[35] H. Chen, Z. Zhang, X. Wang, J. Chen, C. Xu, Y. Liu, Z. Yu, X. Wang, Fabrication of magnetic Fe/Zn layered double oxide@ carbon nanotube composites and their application for U (VI) and 241Am (III) removal, ACS Applied Nano Materials, 1 (2018) 2386-2396.
[36] Q. Yang, S. Wang, F. Chen, K. Luo, J. Sun, C. Gong, F. Yao, X. Wang, J. Wu, X. Li, Enhanced visible-light-driven photocatalytic removal of refractory pollutants by Zn/Fe mixed metal oxide derived from layered double hydroxide, Catalysis Communications, 99 (2017) 15-19.
[37] N. Hashim, M.Z. Hussein, I.M. Isa, A. Kamari, A. Mohamed, M.S. Rosmi, A.M. Jaafar, Layered double hydroxide as a potential matrix for controlled release formulation of phenoxyherbicides, Journal of Science and Mathematics Letters, 4 (2012) 22-36.
[38] W. Muhammad, N. Ullah, M. Haroon, B.H. Abbasi, Optical, morphological and biological analysis of zinc oxide nanoparticles (ZnO NPs) using *Papaver somniferum L*, RSC advances, 9 (2019) 29541-29548.
[39] K. Tharani, L. Nehru, Synthesis and characterization of iron oxide nanoparticle by precipitation method, International Journal of Advanced Research in Physical Science, 2 (2015) 47-50.
[40] L.M. Cao, Y.W. Hu, S.F. Tang, A. Iljin, J.W. Wang, Z.M. Zhang, T.B. Lu, Fe-CoP Electrocatalyst Derived from a Bimetallic Prussian Blue Analogue for Large-Current-Density Oxygen Evolution and Overall Water Splitting, Advanced Science, 5 (2018) 1800949.
[41] D. Xu, D. Fan, W. Shen, Catalyst-free direct vapor-phase growth of $Zn_{1-x}Cu_xO$ micro-cross structures and their optical properties, Nanoscale research letters, 8 (2013) 1-9.
[42] X. Peng, F. Hu, F.L. Lam, Y. Wang, Z. Liu, H. Dai, Adsorption behavior and mechanisms of ciprofloxacin from aqueous solution by ordered mesoporous carbon and bamboo-based carbon, Journal of colloid and interface science, 460 (2015) 349-360.
[43] B. Wang, X. Xu, H. Tang, Y. Mao, H. Chen, F. Ji, Highly efficient adsorption of three antibiotics from aqueous solutions using glucose-based mesoporous carbon, Applied Surface Science, 528 (2020) 147048.
[44] F.P. de Sá, B.N. Cunha, L.M. Nunes, Effect of pH on the adsorption of Sunset Yellow FCF food dye into a layered double hydroxide (CaAl-LDH-NO_3), Chemical Engineering Journal, 215 (2013) 122-127.
[45] R.J. Umpleby, S.C. Baxter, Y. Chen, R.N. Shah, K.D. Shimizu, Characterization of molecularly imprinted polymers with the Langmuir− Freundlich isotherm, Analytical chemistry, 73 (2001) 4584-4591.
[46] S.M. Ibrahim, A.A. Badawy, H.A.J.J.o.N.i.C. Essawy, Improvement of dyes removal from aqueous solution by Nanosized cobalt ferrite treated with humic acid during coprecipitation, 9 (2019) 281-298.
[47] S.M. Ibrahim, A.A. Badawy, H.A. Essawy, Improvement of dyes removal from aqueous solution by Nanosized cobalt ferrite treated with humic acid during coprecipitation, Journal of Nanostructure in Chemistry, 9 (2019) 281-298.
[48] Z.H. Dastgerdi, S.S. Meshkat, M.D. Esrafili, Enhanced adsorptive removal of Indigo carmine dye performance by functionalized carbon nanotubes based adsorbents from aqueous solution: equilibrium, kinetic, and DFT study, Journal of Nanostructure in Chemistry, 9 (2019) 323-334.

[49] S. Maleki, F. Falaki, M. Karimi, Synthesis of SDS micelles-coated Fe3O4/SiO2 magnetic nanoparticles as an excellent adsorbent for facile removal and concentration of crystal violet from natural water samples, Journal of Nanostructure in Chemistry, 9 (2019) 129-139.
[50] S. Carabineiro, T. Thavorn-Amornsri, M. Pereira, J. Figueiredo, Adsorption of ciprofloxacin on surface-modified carbon materials, Water research, 45 (2011) 4583-4591.
[51] Y. Fei, Y. Li, S. Han, J. Ma, Adsorptive removal of ciprofloxacin by sodium alginate/graphene oxide composite beads from aqueous solution, Journal of colloid and interface science, 484 (2016) 196-204.
[52] X. Kong, Y. Liu, J. Pi, W. Li, Q. Liao, J. Shang, Low-cost magnetic herbal biochar: characterization and application for antibiotic removal, Environmental Science and Pollution Research, 24 (2017) 6679-6687.
[53] C.R. Gadipelly, K.V. Marathe, V.K. Rathod, Effective adsorption of ciprofloxacin hydrochloride from aqueous solutions using metal-organic framework, Separation Science and Technology, 53 (2018) 2826-2832.
[54] X. Peng, F. Hu, J. Huang, Y. Wang, H. Dai, Z. Liu, Preparation of a graphitic ordered mesoporous carbon and its application in sorption of ciprofloxacin: kinetics, isotherm, adsorption mechanisms studies, Microporous and Mesoporous Materials, 228 (2016) 196-206.
[55] M.D. Olawale, A.C. Tella, J.A. Obaleye, J.S. Olatunji, Synthesis, characterization and crystal structure of a copper-glutamate metal organic framework (MOF) and its adsorptive removal of ciprofloxacin drug from aqueous solution, New Journal of Chemistry, 44 (2020) 3961-3969.
[56] M.-f. Li, Y.-g. Liu, S.-b. Liu, D. Shu, G.-m. Zeng, X.-j. Hu, X.-f. Tan, L.-h. Jiang, Z.-l. Yan, X.-x. Cai, Cu (II)-influenced adsorption of ciprofloxacin from aqueous solutions by magnetic graphene oxide/nitrilotriacetic acid nanocomposite: competition and enhancement mechanisms, Chemical Engineering Journal, 319 (2017) 219-228.
[57] J. Ma, Y. Sun, M. Zhang, M. Yang, X. Gong, F. Yu, J. Zheng, Comparative study of graphene hydrogels and aerogels reveals the important role of buried water in pollutant adsorption, Environmental science & technology, 51 (2017) 12283-12292.
[58] M. Malakootian, A. Nasiri, H. Mahdizadeh, Preparation of $CoFe_2O_4$/activated carbon@chitosan as a new magnetic nanobiocomposite for adsorption of ciprofloxacin in aqueous solutions, Water Science and Technology, 78 (2018) 2158-2170.
[59] Y. Zhou, S. Cao, C. Xi, X. Li, L. Zhang, G. Wang, Z. Chen, A novel Fe_3O_4/graphene oxide/citrus peel-derived bio-char based nanocomposite with enhanced adsorption affinity and sensitivity of ciprofloxacin and sparfloxacin, Bioresource technology, 292 (2019) 121951.
[60] G.W. Kajjumba, S. Emik, A. Öngen, H.K. Özcan, S. Aydın, Modelling of adsorption kinetic processes—errors, theory and application, in: Advanced sorption process applications, 2018, pp. 0-19.
[61] A. Gürses, Ç. Doğar, M. Yalçın, M. Açıkyıldız, R. Bayrak, S. Karaca, The adsorption kinetics of the cationic dye, methylene blue, onto clay, Journal of Hazardous Materials, 131 (2006) 217-228.
[62] F. Piri, A. Mollahosseini, M.M. Hosseini, Enhanced adsorption of dyes on microwave-assisted synthesized magnetic zeolite-hydroxyapatite nanocomposite, Journal of Environmental Chemical Engineering, 7 (2019) 103338.
[63] S. Lombardo, W. Thielemans, Thermodynamics of adsorption on nanocellulose surfaces, Cellulose, 26 (2019) 249-279.

[64] H.N. Tran, S.-J. You, A. Hosseini-Bandegharaei, H.-P. Chao, Mistakes and inconsistencies regarding adsorption of contaminants from aqueous solutions: a critical review, Water research, 120 (2017) 88-116.
[65] Y.-H. Jia, Z.-H. Liu, Preparation of borate anions intercalated MgAl-LDHs microsphere and its calcinated product with superior adsorption performance for Congo red, Colloids Surfaces A: Physicochemical and Engineering Aspects, 575 (2019) 373-381.
[66] C.A. Demircan, U. Bozkaya, Transition metal cation− π interactions: complexes formed by Fe^{2+}, Co^{2+}, Ni^{2+}, Cu^{2+}, and Zn^{2+} binding with benzene molecules, The Journal of Physical Chemistry A, 121 (2017) 6500-6509.
[67] A. Dementjev, A. De Graaf, M. Van de Sanden, K. Maslakov, A. Naumkin, A. Serov, X-Ray photoelectron spectroscopy reference data for identification of the C_3N_4 phase in carbon–nitrogen films, Diamond related materials, 9 (2000) 1904-1907.
[68] B. Shen, G. Li, F. Wang, Y. Wang, C. He, M. Zhang, S. Singh, Elemental mercury removal by the modified bio-char from medicinal residues, Chemical Engineering Journal, 272 (2015) 28-37.
[69] Y.-J. Zhang, Z.-J. Xing, Z.-K. Duan, M. Li, Y. Wang, Effects of steam activation on the pore structure and surface chemistry of activated carbon derived from bamboo waste, Applied Surface Science, 315 (2014) 279-286.
[70] J. Li, G. Yu, L. Pan, C. Li, F. You, S. Xie, Y. Wang, J. Ma, X. Shang, Study of ciprofloxacin removal by biochar obtained from used tea leaves, Journal of Environmental Sciences, 73 (2018) 20-30.
[71] P. Xuehui, R. Xiangbin, F. KUANG, X. Jiandong, H. Baorong, Inhibiting effect of ciprofloxacin, norfloxacin and ofloxacin on corrosion of mild steel in hydrochloric acid, Chinese Journal of Chemical Engineering, 18 (2010) 337-345.
[72] A.J. Plomp, D.S. Su, K.d. Jong, J.H. Bitter, On the Nature of Oxygen-Containing Surface Groups on Carbon Nanofibers and Their Role for Platinum Deposition An XPS and Titration Study, The Journal of Physical Chemistry C, 113 (2009) 9865-9869.

Declaration of interests

☒ The authors declare that they have no known competing financial interests or personal relationships that could have appeared to influence the work reported in this paper.

☐The authors declare the following financial interests/personal relationships which may be considered as potential competing interests:

Dr. Gaurav Sharma